




University of  
Stavanger

FACULTY OF SCIENCE AND TECHNOLOGY

## MASTER'S THESIS

Study program/specialization: Petroleum Engineering/Natural Gas Engineering	Spring, 2019  Open
Author:  Fawzi Chamssine	 (signature of author)
Supervisor:  Professor Zhixin Yu	
Title of master's thesis:  Catalytic hydrogenation of CO <sub>2</sub> to methanol over In-promoted Cu/ZnO/Al <sub>2</sub> O <sub>3</sub> derived from hydrotalcite-like precursors	
Credits (ECTS): 30	
Key words: CO <sub>2</sub> hydrogenation Methanol Cu-based catalysts Hydrotalcite Indium Kinetic modeling Catalyst characterization	Number of pages: 74  Stavanger, 15/06/2019

## **ACKNOWLEDGEMENTS**

First, I express my endless gratitude and appreciation to my supervisor Professor Zhixin Yu for his professional guidance, continuous support, patience, motivation, enthusiasm, and immense knowledge.

To Kristian Stangeland, Huong Lan Huynh, Dori Yosef Kalai, thank you for all your help. I'm extremely grateful for all your guidance, and support during laboratory work and data analysis.

To Gio, Obinna, Anderson, George, Mohammad and my classmates at the University of Stavanger your support and encouragement pushed me forward throughout this master program.

Finally, to my family in Lebanon. Without you I wouldn't have been here. To my father, my role model and hero, my mother and sister, your endless love and support made me the person I'm today. To that special girl whose been with me through sorrow and joy, thank you.

## ABSTRACT

Carbon dioxide emissions present a threat on a global level, driving governments and the scientific society to search for sustainable solutions to ease the effects of climate change. Carbon utilization offers a potentially effective and environmentally friendly way to lower emissions by recycling carbon dioxide to produce valuable chemicals and fuels. Among these, methanol rises as an important component in the fuel sector as well as in the chemical industry. This creates a large potential for industrial utilization of CO<sub>2</sub> hydrogenation to methanol.

Catalytic hydrogenation of carbon dioxide to methanol is performed using a heterogeneous catalytic system. The commercial Cu/ZnO/Al<sub>2</sub>O<sub>3</sub> catalyst used for methanol synthesis from syngas has been extensively studied due to its relatively high performance and low cost compared to other catalytic systems. However, this catalyst requires improvements to reach the desired efficient industrial standard for CO<sub>2</sub> hydrogenation to methanol. Hydrotalcite-derived Cu/Zn/Al<sub>2</sub>O<sub>3</sub> catalyst has showed promising performance compared to the conventional Cu/ZnO/Al<sub>2</sub>O<sub>3</sub> catalyst for methanol synthesis from CO<sub>2</sub>. Furthermore, it has been demonstrated that promoters (e.g. ZrO<sub>2</sub>, Ga<sub>2</sub>O<sub>3</sub>) can further improve the catalytic performance. Recently, the use of indium oxide has been proposed as a potential material for CO<sub>2</sub> hydrogenation to methanol.

In this study, a series of Cu/ZnO/Al<sub>2</sub>O<sub>3</sub> (CuZnAl) catalysts were prepared via hydrotalcite-like precursors. Different Cu/Zn ratios were implemented using co-precipitation (low saturation) preparation method. Indium (In) promoted catalysts were prepared with the best performing Cu/Zn ratio. The catalysts were characterized by x-ray diffraction, H<sub>2</sub> temperature programmed reduction, and N<sub>2</sub> adsorption-desorption. Hydrotalcite structure was successfully achieved with the formation of CuO and ZnO particles after the calcination process. The addition of In improved CuO dispersion, the reducibility, and textural properties of the catalysts.

Catalytic performance was examined in a fixed-bed reactor at 250°C, 30 bars, and H<sub>2</sub>/CO<sub>2</sub>/N<sub>2</sub> ratio of 3/1/1. A Cu/Zn ratio of 1 resulted in the highest methanol selectivity of 32.3%. The In promotion resulted in lower CO<sub>2</sub> conversion but with a significant improvement in methanol selectivity. The highest methanol selectivity of 52.6% was obtained over the CuZnAl catalyst with an In content of 5 mol%. The superior performance of the In-promoted catalyst was further demonstrated at temperatures of 230°C to 260 °C. Furthermore, long term tests showed that In promotion significantly improved the stability of the catalyst.



# Table of Contents

List of Figures.....	vii
List of Tables .....	ix
1 Introduction.....	1
1.1 Background.....	1
1.2 Scope of study.....	3
2 CO <sub>2</sub> hydrogenation to methanol.....	4
2.1 Thermodynamics of methanol synthesis .....	4
2.2 Methanol synthesis catalysts .....	5
2.2.1 Copper-based catalyst .....	5
2.2.2 Zinc oxide-based catalysts.....	13
2.2.3 Indium oxide-based catalysts .....	13
2.3 Other catalytic systems for CO <sub>2</sub> hydrogenation to methanol.....	15
2.4 Catalyst synthesis.....	17
2.4.1 Catalyst synthesis by co-precipitation.....	17
2.4.2 Aging.....	19
2.4.3 Calcination.....	19
2.4.4 Reduction.....	19
2.5 Catalyst characterization .....	19
2.5.1 X-ray diffraction (XRD).....	19
2.5.2 Temperature programmed reduction.....	20
2.5.3 Nitrogen adsorption-desorption.....	21
2.5.4 Gas chromatography .....	22
2.6 Kinetics of methanol synthesis .....	23
2.6.1 Kinetic models.....	23
2.6.2 Power Law model .....	24
3 Experimental .....	28
3.1 Materials and equipment .....	28
3.2 Catalyst synthesis.....	28
3.3 Characterization of catalysts.....	29
3.3.1 X-ray diffraction (XRD).....	29
3.3.2 Temperature programmed reduction (TPR).....	30
3.3.3 Nitrogen adsorption – desorption .....	30
3.4 Catalytic Activity Tests.....	30
4 Results and discussion.....	33

4.1	Characterization of catalysts.....	33
4.1.1	XRD analysis of un-promoted catalysts.....	33
4.1.2	XRD analysis of promoted catalysts.....	35
4.1.3	TPR analysis.....	37
4.1.4	N <sub>2</sub> adsorption-desorption.....	39
4.2	Methanol synthesis activity tests.....	41
4.2.1	Activity and selectivity of un-promoted catalysts.....	41
4.2.2	Activity and selectivity of promoted catalysts.....	42
4.2.3	Temperature effect on the 1-CuZnAl-5-In and 1-CuZnAl-0-In catalysts.....	43
4.2.4	Long run reactions.....	45
5	Conclusions and future work.....	47
5.1	Conclusions.....	47
5.2	Recommendations for future work.....	48
6	References.....	49
	APPENDIX A: CALCULATIONS OF CATALYSTS SYNTHESIS.....	64

## List of Figures

Figure 1.1. Global methanol industry demand in different geographical areas [10] .....	2
Figure 2.1. Carbon oxide conversion as a function of temperature. A: 100 Bar, B: 75 Bar, C: 50 Bar [24].....	4
Figure 2.2. Effect of pressure and temperature on (a) CO <sub>2</sub> conversion and (b) methanol selectivity at phase and chemical equilibrium. Dashed lines represent the chemical equilibrium predicted by gas-phase thermodynamics [26] .....	5
Figure 2.3. Reaction mechanism of methanol synthesis over Cu (111)[29] .....	6
Figure 2.4. Crystal structure of UiO-66 having ZrO <sub>3</sub> secondary building units linked with BDC (1,4-benzenedicarboxylate) to form an array [48] .....	9
Figure 2.5. Chemical synthesis of UiO-bpy via insitu reduction [49] .....	10
Figure 2.6. a) Space time yield (STY) of methanol vs reaction time on stream (100 h) b) Selectivity of product vs reaction time reaction time [49]. .....	10
Figure 2.7. Mechanism of active oxygen sites on In <sub>2</sub> O <sub>3</sub> (110) surface [71] .....	14
Figure 2.8. Preparation method of Pd/In <sub>2</sub> O <sub>3</sub> catalyst using Pd peptide composition and In <sub>2</sub> O <sub>3</sub> powder [20].....	14
Figure 2.9. Schematic illustration of layered double hydroxide structure and chemical components [99].....	18
Figure 2.10. (a) Types of physisorption isotherms (b) Types of hysteresis loops [113] .....	22
Figure 2.11. Example of parity plot representation of methanol synthesis (a) and Reverse Water Gas Shift Reaction (b) [121].....	27
Figure 3.1. Schematic representation of the experimental set up .....	31
Figure 4.1. XRD patterns of un-promoted as-prepared catalysts, (▲) ZnO and (●) CuO.....	33
Figure 4.2. XRD patterns of un-promoted calcined catalysts, (▲) ZnO and (●) CuO.....	35
Figure 4.3. XRD patterns of promoted as-prepared catalysts, (*) In (OH) <sub>3</sub> .....	36
Figure 4.4. XRD patterns of promoted calcined catalysts, (▲) ZnO and (●) CuO.....	37
Figure 4.5. TPR profiles of calcined catalysts .....	38
Figure 4.6. N <sub>2</sub> adsorption-desorption isotherms of calcined catalysts .....	39
Figure 4.7. Pore size distribution of calcined catalysts .....	40
Figure 4.8. CO <sub>2</sub> conversion and CH <sub>3</sub> OH selectivity of CuZnAl catalysts .....	41
Figure 4.9. CO <sub>2</sub> conversion and CH <sub>3</sub> OH selectivity of promoted CuZnAl catalysts .....	43
Figure 4.10. Effect of temperature on CO <sub>2</sub> conversion and CH <sub>3</sub> OH selectivity on 1-CuZnAl-5-In and 1-CuZnAl-0-In catalysts .....	44

Figure 4.11. CO<sub>2</sub> conversion and methanol selectivity over the 1-CuZnAl-5-In catalyst for 72 h TOS. The black lines indicate the average CO<sub>2</sub> conversion and methanol selectivity of the last 1 hour. .... 46



## List of Tables

Table 2.1. Selected results of Cu-based catalysts .....	12
Table 2.2. Summary of selected catalysts .....	16
Table 2.3. Ionic radii of cations [90] .....	18
Table 3.1. List of used chemicals for catalyst preparation and gases for activity tests. ....	28
Table 3.2. Labels and characteristics of the prepared catalysts .....	29
Table 3.3. Specs of the reactor bed .....	32
Table 4.1. Structural parameters of un-promoted as-prepared catalysts and calculated crystallite size .....	34
Table 4.2. Structural parameters of promoted as-prepared catalysts and calculated crystallite size .....	36
Table 4.3. Textual properties of calcined catalysts .....	40
Table 4.4. Summary of average CO <sub>2</sub> conversion and CH <sub>3</sub> OH selectivity of un-promoted catalysts .....	42
Table 4.5. Summary of average CO <sub>2</sub> conversion and CH <sub>3</sub> OH selectivity of promoted catalysts .....	43
Table A 1. Stoichiometric coefficients of CuZnAl catalysts .....	64
Table A 2. Mass of salts used .....	64
Table A 3. Stoichiometric coefficients of CuZnAl-In catalysts .....	65
Table A 4. Mass of salts used .....	65

# 1 Introduction

## 1.1 Background

Carbon dioxide (CO<sub>2</sub>) discharge is one of the main drivers of the enhanced greenhouse effect which relates to the global climate change epidemic faced today. The international community and local governments are working on implementing strict environmental laws and international treaties, trying to decrease the global CO<sub>2</sub> emission levels. It is predicted that CO<sub>2</sub> emissions have to be reduced by a minimum of 50% by the year 2050 to limit global temperature increase to an average of 2°C [1]. CO<sub>2</sub> is emitted in almost every industry whether from direct emissions or energy usage. In 2018, global CO<sub>2</sub> emissions were estimated to be 37.1 Gt, a 2.7% increase from 2017 [2]. Various methods can contribute significantly in reducing the amount of CO<sub>2</sub> in the atmosphere such as carbon capture and storage (CCS). CCS can be applied to capture CO<sub>2</sub> from commercial and industrial plants, which is then transported and finally injected into a safe underground storage, where depleted oil and natural gas fields are usually used as storage sites [3]. CCS faces specific limitations such as high implementation costs, transport methods, and scarcity in suitable geological locations for storage [4]. Thus, CO<sub>2</sub> utilization technologies rise as a possible solution to further reduce CO<sub>2</sub> emissions. This can have a positive economic impact on the cost of reducing the emissions.

In 2005, George A. Olah introduced a model named “The Methanol Economy” [5]. This model was proposed as an alternative to the hydrogen economy and was centered around green methanol synthesis and utilization. Methanol (CH<sub>3</sub>OH) is one of the several liquid fuels that can be synthesized from CO<sub>2</sub>, which serves as a suitable energy storage medium and a feedstock for several industries. In addition, it can contribute to the transition from fossil fuels to renewable energy due to its high efficiency when it comes to energy production [6]. Methanol is recognized as an efficient manner of energy storage, since it has high energy density by volume and weight. Besides, it does not require high pressure to store at room temperature, which makes it safer to handle [7]. Methanol is also applicable in internal combustion engines (ICE) as it has excellent combustion characteristics. It possesses a higher-octane rate, and only half of the energy density of gasoline. Gasoline cars can be easily modified to run on methanol, or a methanol – gasoline mixture at low cost. For instance, 80% of the cars manufactured in Brazil today are so-called “Flexible Fuel Vehicles”, meaning that they are able to run on any mixture of gasoline and ethanol (ethanol because of the abundance of sugar canes at low cost) [8]. Furthermore, in 2012 the Chinese government ran a pilot test

initiative to verify methanol’s efficiency as an alternative fuel. The results showed positive prospects of methanol engines (M100) and industrial guidelines concerning safety, management, and construction of methanol fuelling stations were established. On 19 March 2019, Chinese ministries and key government agencies endorsed a methanol vehicle policy to be implemented on a national level. In the five years coming, it is expected that 50,000 M100 vehicles (buses, trucks, and cars) will be in use, with a methanol consumption exceeding 500,000 million metric tons per annum [9]. As demonstrated in Figure 1.1, global methanol industry demand is increasing because of its use in fuel blends and as an industrial feedstock. Thus, developing more efficient synthesis technologies and methods as well as alternative routes to produce methanol is highly attractive.

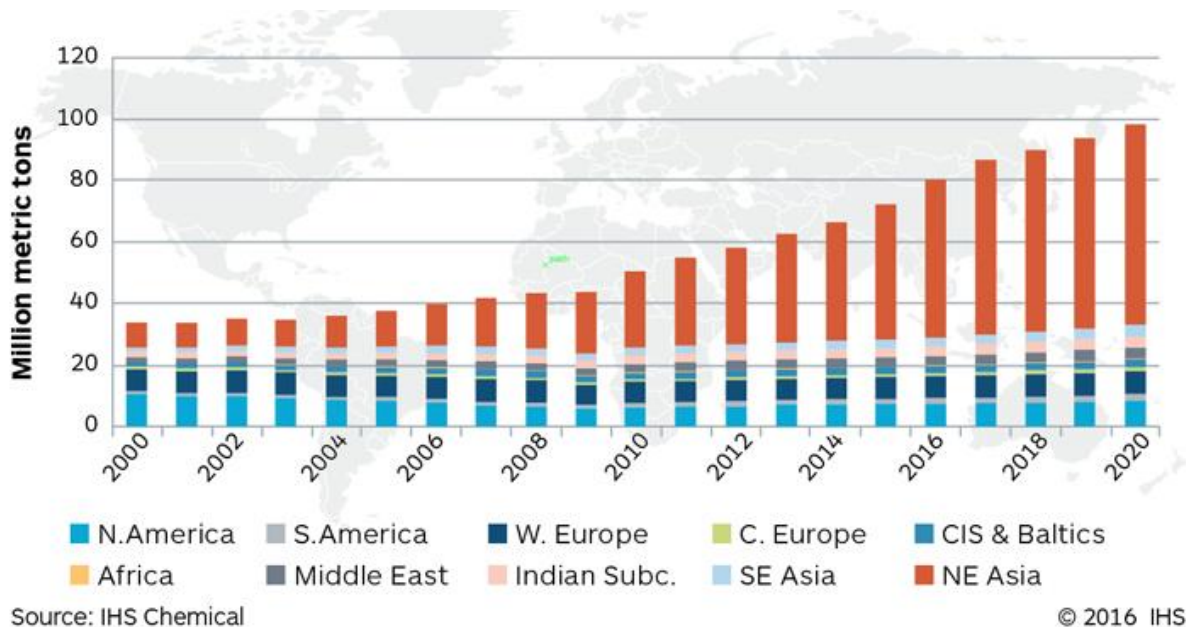


Figure 1.1. Global methanol industry demand in different geographical areas [10]

Methanol synthesis can be done by different processes and different carbon sources. However CO<sub>2</sub> is considered as beneficial on multiple levels [11]. Thus, a significant interest has been shown towards catalytic hydrogenation of CO<sub>2</sub>, which can yield a range of different products, such as methane, formaldehyde, formic acid, carbon monoxide, and methanol [12, 13].

Heterogeneous catalytic systems for hydrogenation of CO<sub>2</sub> to methanol have been under extensive investigation over the past decade. It is widely acknowledged that copper (Cu) is highly active for CO<sub>2</sub> hydrogenation to methanol [14]. Studies show that Cu-based catalysts perform better with the incorporation of different supports/promoters to achieve better catalytic performance, since copper by itself is inefficient [15]. The common industrial catalyst used for

syngas conversion to methanol is Cu/ZnO/Al<sub>2</sub>O<sub>3</sub>. This catalytic system is widely studied for CO<sub>2</sub> hydrogenation to methanol, but it suffers from moderate catalytic performance and deactivates quickly due to water induced sintering [16]. This has given rise to the search for new catalytic systems that achieve better activity, methanol selectivity, and stability. Hydrotalcite-like components obtained from hydrotalcite precursors show promising properties compared to conventional material such as high stability, H<sub>2</sub> yield, and low CO production [17]. Different promoters have been examined for Cu/ZnO based catalysts over the last decades. Indium oxide-based catalyst has shown promising stability and high methanol selectivity even at high temperatures [18-21]. Therefore, In rises as a promising metal to enhance methanol selectivity and catalytic stability of the commercial Cu/ZnO/Al<sub>2</sub>O<sub>3</sub> catalyst.

## **1.2 Scope of study**

In this study, a series of Cu/ZnO/Al<sub>2</sub>O<sub>3</sub> (CuZnAl) catalysts with different Cu/Zn ratios (Cu/Zn = 0.5, 1.0 and 1.5) were prepared through a hydrotalcite-like precursor. In addition, In-promoted catalysts were prepared with a fixed Cu/Zn ratio of 1. The catalysts were characterized by XRD, H<sub>2</sub>-TPR, and N<sub>2</sub> adsorption-desorption. The catalytic performance for CO<sub>2</sub> hydrogenation to methanol was also investigated. In addition, temperature effect tests and long-term tests were conducted on the best performing promoted catalyst to further investigate the stability and the performance of the catalyst.

## 2 CO<sub>2</sub> hydrogenation to methanol

### 2.1 Thermodynamics of methanol synthesis

CO<sub>2</sub> is a thermodynamically stable, highly oxidized compound having a low reactivity and therefore, it is necessary to overpass a thermodynamic barrier in order to activate CO<sub>2</sub> [22]. Thus, conversion of CO<sub>2</sub> requires effective reaction conditions, high energy input, and suitable active catalysts.

Thermochemical methanol synthesis in a catalytic reactor is composed of two main hydrogenation reactions and one side reaction, which is the reverse water gas shift reaction (RWGS) [23]. The reactions are expressed below:



Reactions (1) and (2) are exothermic while reaction (3) is an endothermic reaction. In addition, methanol synthesis results in a decrease in mole number. Consequently, according to Le Chatelier's principle, the maximum conversion of CO<sub>2</sub> is obtained at high pressure and low temperature as indicated in Figure 2.1 [24].

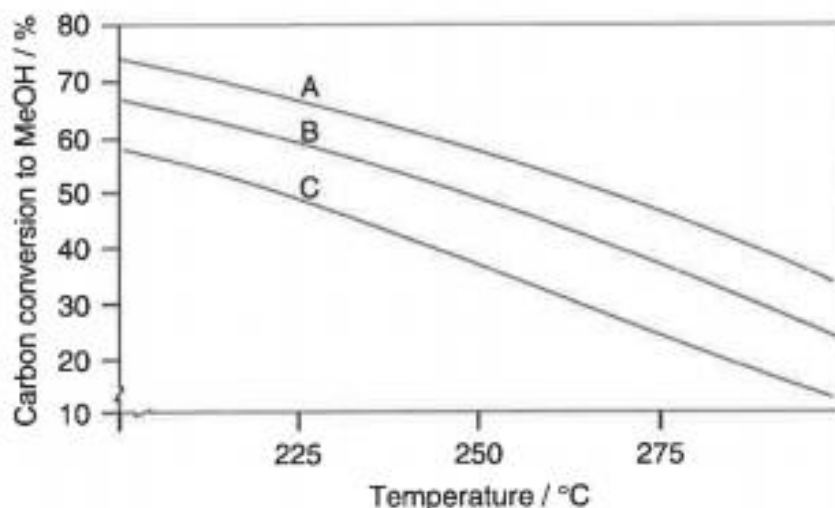


Figure 2.1. Carbon oxide conversion as a function of temperature. A: 100 bars, B: 75 bars, C: 50 bars [24]

The increase in reaction temperature improves significantly the kinetics of methanol synthesis (activation of CO<sub>2</sub> is promoted), while it also results in reduction of methanol selectivity, since

the endothermic RWGS reaction becomes more prominent [25]. Figure 2.2 shows the CO<sub>2</sub> conversion and methanol selectivity at different pressures and temperatures taking into account an H<sub>2</sub>/CO<sub>2</sub> feed of 3/1 stoichiometric molar ratio [26]. As can be seen, pressure and temperature contribute significantly in the equilibrium conversion of CO<sub>2</sub>. The implementation of highly selective catalyst is crucial for methanol production process, since other products such as higher alcohols and hydrocarbons are also thermodynamically favorable at these conditions.

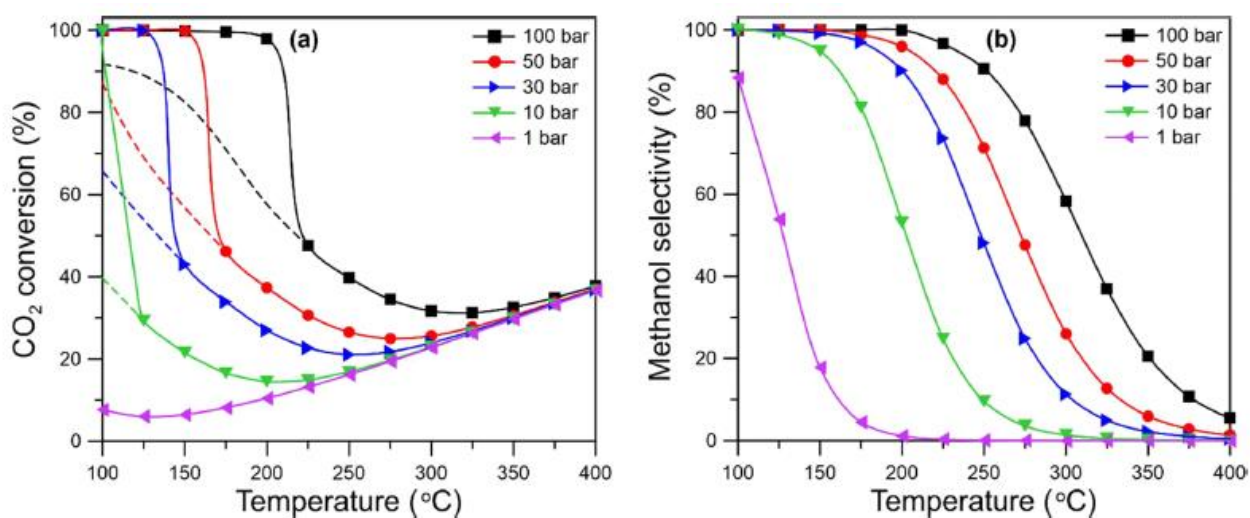


Figure 2.2. Effect of pressure and temperature on (a) CO<sub>2</sub> conversion and (b) methanol selectivity at phase and chemical equilibrium. Dashed lines represent the chemical equilibrium predicted by gas-phase thermodynamics [26]

## 2.2 Methanol synthesis catalysts

### 2.2.1 Copper-based catalyst

During the past decade, CO<sub>2</sub> hydrogenation was under extensive theoretical and experimental investigation [27]. Methanol synthesis from CO<sub>2</sub> requires a catalytic system that can offer high selectivity towards methanol, high activity, and limits the production of bi-products. Currently, the commercial catalyst used in methanol synthesis from syngas is comprised of copper, zinc oxide, and aluminum oxide (Cu/ZnO/Al<sub>2</sub>O<sub>3</sub>). This catalytic system has also been extensively studied for CO<sub>2</sub> hydrogenation to methanol, but it requires improvements in methanol selectivity, activity, and stability to meet industrial requirements [28].

### 2.2.1.1 Reaction mechanism on Cu (111)

The reaction mechanism on Cu has been determined by various studies and the “Density Functional Theory” (DFT). Figure 2.3 demonstrates two major routes which have been proposed to methanol synthesis over a clean Cu (111) based catalyst.

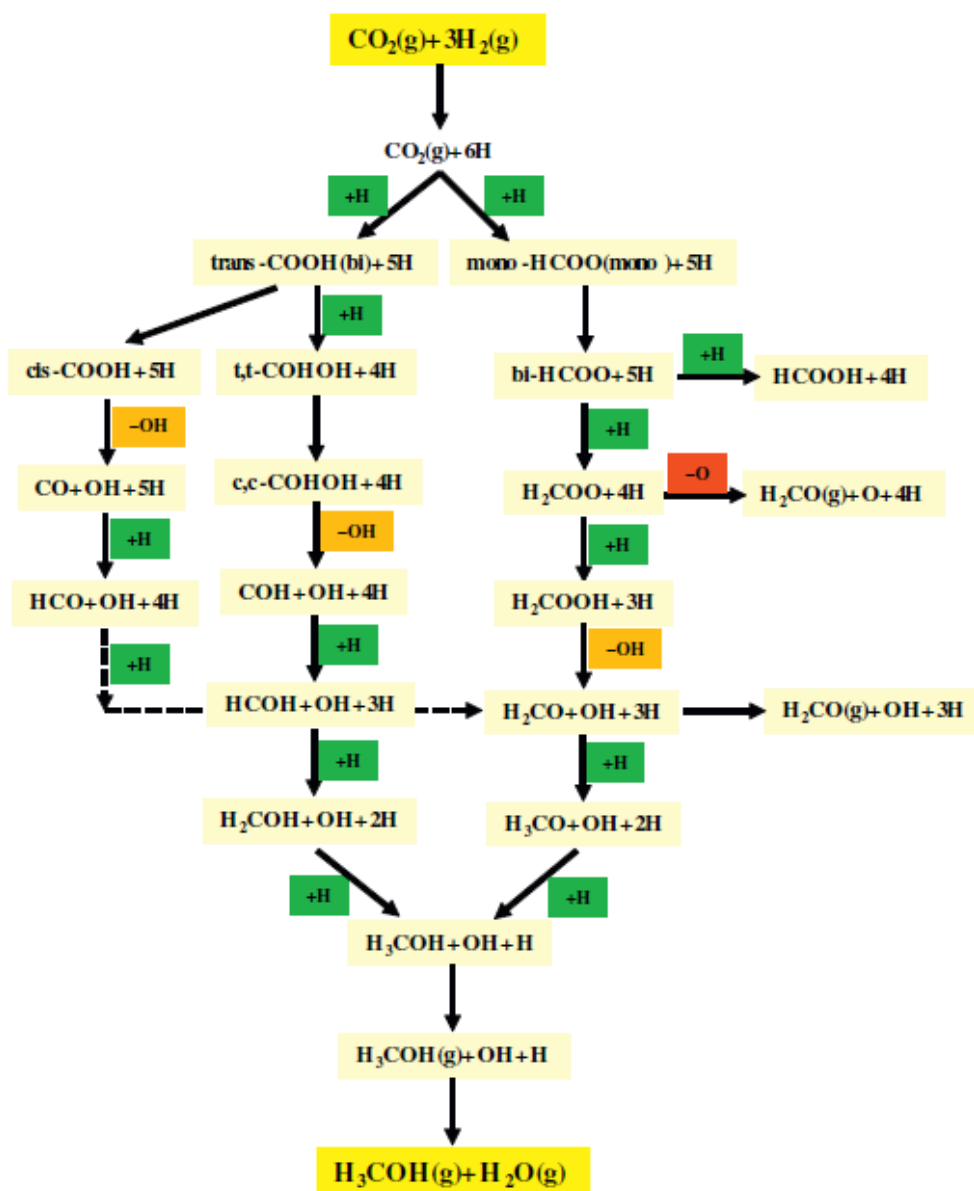


Figure 2.3. Reaction mechanism of methanol synthesis over Cu (111)[29]

The pathway to the right shows the formation of intermediate formate (HCOO) with a surface H atom. Afterwards HCOO is hydrogenated to dioxymethylene (HCOOH), followed by hydrogenation to form  $\text{H}_2\text{COOH}$ , which disassociates into formaldehyde ( $\text{H}_2\text{CO}$ ) and hydroxyl (OH). The  $\text{H}_2\text{CO}$  is hydrogenated into  $\text{H}_3\text{CO}$  (methoxy) or  $\text{H}_2\text{COH}$  (methylenoxy), and the final product is methanol.

The second path shows the formation of trans-carboxyl group (COOH). Adsorbed COOH can exist in two isomer structures; cis and trans-COOH, which have the H atom points upwards from the surface in cis and towards the surface in trans [29]. Trans-COOH is hydrogenated to form t,t-COHOH, the isomer of adsorbed dihydrocarbene. This path is slightly exothermic having an activation barrier of 0.43 eV. During this path three inter-conventional pathways are formed t,t-COHOH→t,c-COHOH→c,c-COHOH. Afterwards, c,c-COHOH is decomposed to form COH and OH. Then HCO is formed through hydrogenation of CO. Further hydrogenation will lead to the formation of HCOH which is an exothermic reaction [14].

Similarly, in the cis-COOH path it is decomposed into CO + OH. Then HCO is formed by hydrogenation of CO. Further hydrogenation will lead to the formation of HCOH, an endothermic reaction, which will re-unite the path with the trans-COOH path. It is noted that the exothermic formation of HCOH is more favoured kinetically since it has a lower energy barrier of 0.44 eV compared to the endothermic path of energy barrier 1.06 eV. Then, two reaction paths are recognized for the formation of H<sub>2</sub>COH formation. H<sub>2</sub>COH can be produced by the hydrogenation of HCOH in a Langmuir-Hinshelwood (LH) mechanism, or by Eley-Rideal (ER) mechanism. Then H<sub>2</sub>COH is hydrogenated to form methanol, which is a highly exothermic reaction, with an energy barrier of 0.62 eV. Compared to the H<sub>3</sub>CO hydrogenation with a barrier of 0.9 eV, the H<sub>2</sub>COH pathway is more favourable. But since the dominant HCOO is a mechanistic dead end, because of the unstable nature of HCOO and its high tendency to form unwanted bi-products, thus the catalyst can be deactivated due to HCOO poisoning [29].

Furthermore, the presence of water can lead to sintering of the Cu and ZnO phases, which deactivates the catalyst [30, 31]. In addition, Zhao *et al.* [29] conducted a DFT study to examine the role of H<sub>2</sub>O in methanol synthesis. The presence of water on the catalytic surface may poison the active sites and decrease the methanol formation rate. However, it was found that the presence of water promotes trans-COOH formation which is a main intermediate in the formation of COOH in the hydrocarboxyl mechanism. Moreover, the presence of H<sub>2</sub>O on the catalyst's surface contributes in the formate mechanism by hindering further decomposition or hydrogenation of HCOO to methanol [29].

### **2.2.1.2 Metal oxides supports**

Modification and tuning of catalysts can be controlled by introducing a proper support, where the stabilization of active phases, formation of active phases, and the interactions between main catalytic components can be enhanced. Focus of current research is being done on Cu/ZnO and



various other modified catalysts in industrial and theoretical research applications [32]. ZnO has been an attractive support, given the fact that it enhances the lattice oxygen vacant sites, the stability, and dispersion of Cu, and carries an active electron pair towards methanol synthesis [33]. The Cu/ZnO relatively high performance proposed several theories regarding the mechanism between Cu and ZnO. Rhodes and Bell [34], and Fisher and Bell [35] suggested a widely accepted double-site mechanism where Cu sites were suggested to be responsible for hydrogen adsorption and disassociation, while the adsorption of CO<sub>2</sub> occurs on the ZnO site. Thus, the hydrogen atoms migrate from the Cu surface to the ZnO to gradually hydrogenate CO<sub>2</sub> into methanol.

In order to increase efficiency of Cu/ZnO catalysts, more modifications can be done by adding a variety of stabilizers and promoters. Toyir *et al.* [36], examined the effect of gallium oxide (Ga<sub>2</sub>O<sub>3</sub>) where the small particle size favoured the creation of an intermediate phase of Cu between Cu<sup>0</sup>, Cu<sup>2+</sup>, and to some extent Cu<sup>+</sup>. Li *et al.*[37], suggested that the addition of Ga<sup>3+</sup> to the Cu/ZnO catalyst's precursor fastened the reduction of ZnO to Zn<sup>0</sup> through the formation of an "electronic heterojunction of ZnO-MGa ( M= Cu or Zn)", where CuZn is formed by the interaction between reduced Zn<sup>0</sup> and Cu nanoparticles. Thus, the activity and selectivity to methanol is enhanced by the formation of a CuZn bi-metallic active phase on the catalyst's interface. In addition, Martin *et al.* [38] discovered the effect of introducing little amounts of noble metals which contributed in increasing stability of interaction between Cu and Zn and stimulated electronic stability of Cu<sup>0</sup>.

Aluminium oxide (Al<sub>2</sub>O<sub>3</sub>) has frequently been regarded as a structural promoter to increase activity and stability of Cu/ZnO [14, 39]. Kuhl *et al.*[40], demonstrated a hydrotalcite (HT) derived Cu/ZnO/Al<sub>2</sub>O<sub>3</sub> catalyst which was more active than the conventional catalyst. Furthermore, the addition of fluorine ions was suggested by Gao *et al.* [41-43]. Fluorine enhanced the adsorption of CO<sub>2</sub>, and the basicity of Cu/ZnO/Al<sub>2</sub>O<sub>3</sub> that resulted in increased methanol selectivity. In addition, a study also by Gao *et al.*[44] showed that appropriate amounts of yttrium (Y) could improve the catalyst performance by increasing dispersion and surface area of Cu, however weaken ZnO and Cu interaction. Furthermore, the addition of small amounts of both Zr and Y could enhance methanol yield [45].

On the other hand, zirconia (ZrO<sub>2</sub>) has been recognized as a superior promoter or support for methanol synthesis catalyst since the addition of ZrO<sub>2</sub> can increase Cu dispersion, and surface area. The performance of Cu/ZrO<sub>2</sub> catalyst can also be affected by the ZrO<sub>2</sub> crystal structure [14]. Samson *et al.* [46] investigated a Cu/ZrO<sub>2</sub> catalyst and found that oxygen vacancy sites

in t-ZrO<sub>2</sub> (t = tetrahedral) enhance methanol selectivity and yield by promoting Cu particles into the ZrO<sub>2</sub> lattice phase with the development of stable Cu<sup>0</sup>. Ro *et al.* [47], conducted methanol synthesis from CO<sub>2</sub> hydrogenation over catalysts prepared by the controlled surface reactions method (CSR) and atomic layer deposition approaches. The formation of interfacial sites of Cu-ZrO<sub>2</sub> increased the turnover frequency factor in methanol synthesis. Measurement of x-ray adsorption near edge structures (XANES) verified that Cu<sup>0</sup> and Zr<sup>4+</sup> are the primary oxidation states of Cu and Zr. However, it was suggested that some of the Cu atoms diffused into the ZrO<sub>2</sub> structure to create a Cu-ZrO<sub>x</sub> interface, where the valence state of Cu and Zr was Cu<sup>+</sup> and Zr<sup>3+</sup> (a < 4). Rungtaweeworanit *et al.* [48] conducted a study on a Cu@UiO-66 catalyst where UiO-66 is a Zr constructed metal organic frameworks (MOF) as shown in Figure 2.4. Characterization results proved a strong interaction between the ZrO in the secondary structured unit of UiO-66 and Cu particles, thus more active sites were formed leading to better catalytic performance towards methanol compared to the conventional Cu/ZnO/Al<sub>2</sub>O<sub>3</sub> catalyst. In addition, another study of methanol synthesis using MOFs have been done by An *et al.* [49]. Building units of Zr<sub>6</sub>(μ<sub>3</sub>-O)<sub>4</sub>(μ<sub>3</sub>-OH)<sub>4</sub> sites were pre-assembled on a UiO-bipyridine (bpy) MOF, in order to fix Cu/ZnO<sub>x</sub> nanoparticles (Figure 2.5). Cu/ZnO<sub>x</sub>@UiO-bpy catalyst demonstrated high selectivity to methanol and space time yield compared to the conventional Cu/ZnO/Al<sub>2</sub>O<sub>3</sub> catalyst (Figure 2.6).

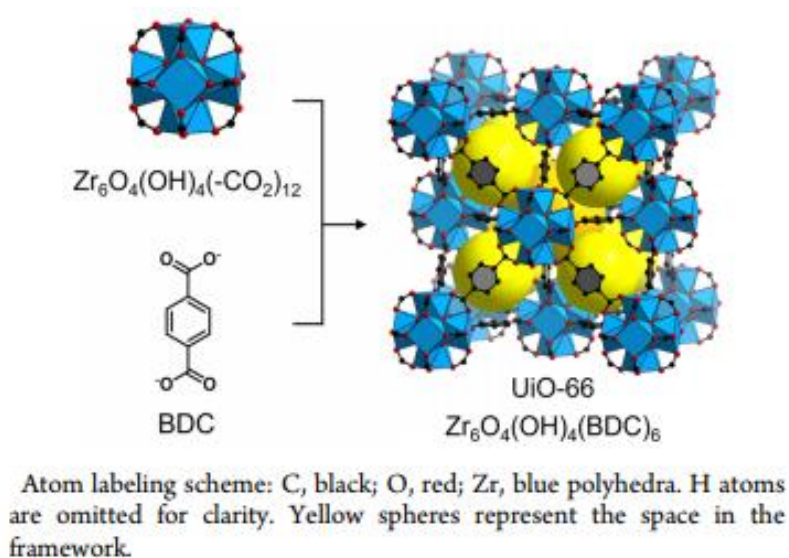


Figure 2.4. Crystal structure of UiO-66 having Zr secondary building units bind with BDC (1,4-benzenedicarboxylate) to form an array [48]

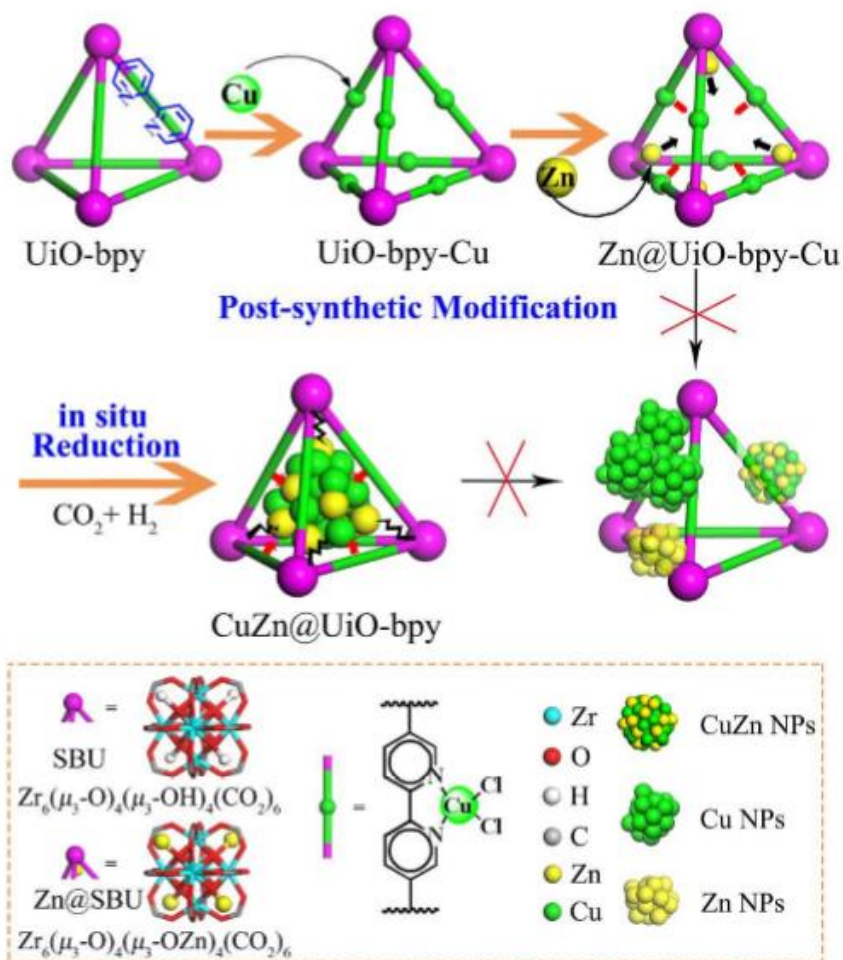


Figure 2.5. Chemical synthesis of UiO-bpy via *insitu* reduction [49]

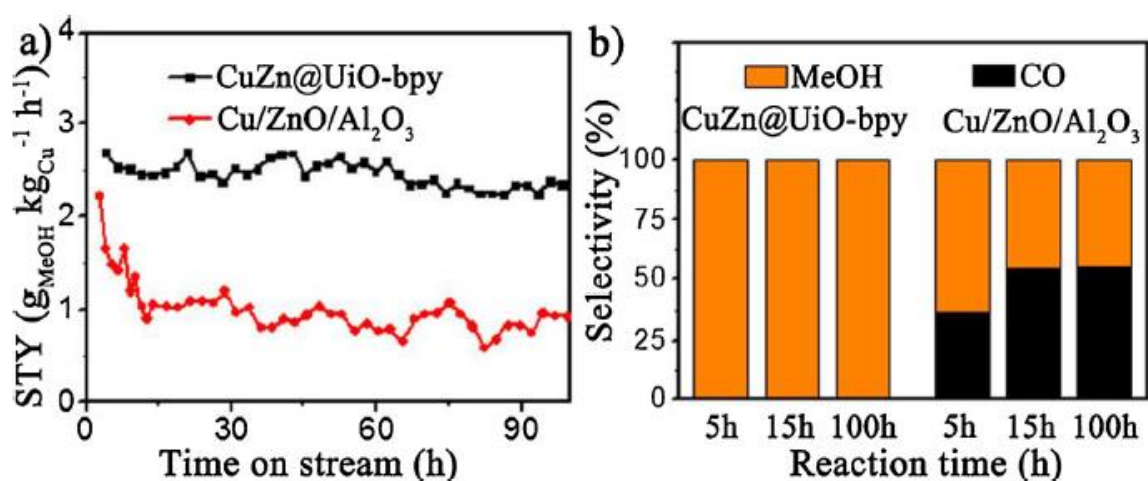


Figure 2.6. a) Space time yield (STY) of methanol vs reaction time on stream (100 h) b) Selectivity of product vs reaction time reaction time [49].

The activity and stability of Cu/ZrO<sub>2</sub> can be improved by modifying preparation methods or by introducing specific additives. Gallium (Ga) was examined in the form of Ga<sub>2</sub>O<sub>3</sub> implemented as a promoter for a catalyst with ZrO<sub>2</sub> support. As a result, the catalyst became 5 times more active to methanol production due to an enhancement in methanol selectivity [50]. Furthermore, the vapor chemical deposition of zirconium tert-butoxide (Zr(O-tBu)<sub>4</sub>) on Cu was found to enhance catalytic synergy between Cu and the ZrO<sub>x</sub>H<sub>y</sub> over-layer found in the sub-monolayer structure which increased CO<sub>2</sub> selectivity that contributed in H<sub>2</sub>O activation over the ZrO<sub>x</sub>H<sub>y</sub> structure [51].

High activity catalysts were produced by deposition of cerium oxide (CeO<sub>x</sub>) and ZnO nanoparticles over Cu (111) [52, 53]. In these studies, CeO<sub>x</sub>/Cu (111) had less activation energy for CO<sub>2</sub> conversion to methanol than ZnO/Cu (111). This can be attributed to the formation of stable carboxyl intermediates on the interface of Cu and CeO<sub>x</sub>, which indicates that the oxide/metal structure could decrease the reaction barriers.

Titanium oxide (TiO) has also been demonstrated to achieve relatively high catalytic performance in CO<sub>2</sub> hydrogenation to methanol. A Cu/TiO catalyst developed by Bao *et al.* [54] indicated that Ti<sup>3+</sup> could enhance CO<sub>2</sub> activation/adsorption thus leading to larger Cu crystals and small surface area. Chen *et al.* [55] implemented lanthanum oxide (LaO<sub>x</sub>) to study the effect of Cu-LaO<sub>x</sub> interface. Notably, the catalyst synthesis was done over a La-modified SBA-15 mesoporous structure to enhance and maximize Cu-LaO<sub>x</sub> interface. The catalyst showed significant improvement in activity and methanol selectivity compared to the commercial Cu/ZnO/Al<sub>2</sub>O<sub>3</sub> catalyst.

### 2.2.1.3 Other Cu-based catalysts

Other materials have been used as metal supports which have showed great potential for improving the performance of Cu-based catalysts in CO<sub>2</sub> hydrogenation to methanol. Vidal *et al.* [56] studied the efficiency of titanium carbide (TiC(100)) where Cu particles were placed over a TiC(100) surface. This created charge polarization of Cu which promoted the activity of CO<sub>2</sub> and methanol synthesis. The binding energy of CO<sub>2</sub> was much larger than Cu (111), suggesting that metal carbides can act as efficient support for methanol synthesis. A study by Kunkel *et al.* [57] presented transition metal carbides (TMC) (TM = Zr, Ti, Nb, Hf, Ta, Mo) for CO<sub>2</sub> capturing and activation, which showed high potential of CO<sub>2</sub> activated adsorption. Kunkel's work inspired Posada-Perez *et al.* [58], to use TMCs as a support on Cu in methanol synthesis. Their work was focused on molybdenum (Mo), and the results showed that methanol synthesis followed a different reaction pathway than on conventional Cu/ZnO catalysts. This

new pathway indicated that Cu/MoC worked as a bifunctional catalytic system, where Cu clusters decomposed CO<sub>2</sub> into CO and O, while MoC and Cu supported clusters contributed in the methanol formation by promoting hydrogenation.

Branco *et al.* [59] suggested that *f*-block bimetallic oxide elements could be an effective addition to the Cu-based catalyst. The catalyst demonstrated higher activity by 2-9 times with comparison to the commercial Cu/ZnO/Al<sub>2</sub>O<sub>3</sub> catalyst, with a high methanol selectivity (>90%). The use of carbon nanotubes (CNTs) was studied by Wang *et al.*[60] and Sun *et al.* [61]. They concluded that the presence of nitrogen containing groups can boost the dispersion of copper oxides (CuO) where Cu particle size decreased, and CO<sub>2</sub> and H<sub>2</sub> adsorption on surface was enhanced. A graphene supported Cu-ZnO catalyst was studied by Deerattrakul *et al.* [62]. The catalyst showed that Cu and Zn species oxidation state was close to Cu<sup>0</sup> and Zn<sup>2+</sup>, however the catalytic performance was highly dependent on the preparation method of the reduced graphene aerogel (rGOae). A selection of Cu-based catalysts is listed in Table 2.1 showing their different performance from literature.

Table 2.1. Selected results of Cu-based catalysts

Catalysts	Temperature (C°)	Pressure (Bar)	H <sub>2</sub> /CO <sub>2</sub> molar ratio	CO <sub>2</sub> conversion (%)	CH <sub>3</sub> OH selectivity (%)	Ref.
Cu/ZnO	250	30	3/1	~11.0	–	[63]
Cu/ZrO <sub>2</sub>	260	80	3/1	15	86	[47]
CuO/ZnO	250	20	3/1	8.6	45	[64]
Cu/ZnO/Al <sub>2</sub> O <sub>3</sub>	270	50	3/1	23.7	43.7	[42]
Cu/ZnO/Al <sub>2</sub> O <sub>3</sub> /ZrO <sub>2</sub>	190	50	3/1	10.7	81.8	[65]
Cu/ZnO/Al <sub>2</sub> O <sub>3</sub> /Y <sub>2</sub> O <sub>3</sub>	230	90	3/1	29.9	89.7	[44]
Cu/ZnO/ZrO <sub>2</sub> /Al <sub>2</sub> O <sub>3</sub> /SiO <sub>2</sub>	250	50	2.8/1	–	99.72	[36]
Cu/ZnO/Ga <sub>2</sub> O <sub>3</sub>	240	45	2.8/1	27	50	[37]
Cu/TiO <sub>2</sub>	260	30	3/1	–	64.7	[54]
Cu/LaO <sub>x</sub> -SBA	240	30	3/1	6	80	[55]
Cu/ZrO <sub>2</sub> /CNTs	260	30	–	16.3	43.5	[60]
CnZnO@UiO-bpy	250	40	3/1	3.3	100	[49]
CuZnO/rGOae	250	15	3/1	–	–	[62]

### 2.2.2 Zinc oxide-based catalysts

ZnO was first used by Waugh *et al.* [66] in 1923 under a pressure of 200 Bar and temperature of 400°C. Liu *et al.* [67] studied methanol synthesis using ZnGa<sub>2</sub>O<sub>4</sub> combined with a molecular sieve SAPO-34 (zeolites) in order to obtain direct conversion from CO<sub>2</sub> to low olefins. A ZnO/Cr<sub>2</sub>O<sub>3</sub> catalyst was studied by Song *et al.* [68] where the catalyst showed high activity towards methanol synthesis, however this catalyst was mainly studied in methanol synthesis using CO rather than CO<sub>2</sub> hydrogenation. Recently, a ZnO-ZrO<sub>2</sub> solid solution was suggested by Wang *et al.* [69], where it showed a high resistance to sulfur poisoning compared to other metallic supported catalysts. The catalyst demonstrated high selectivity towards methanol between 86%-91% and a CO<sub>2</sub> conversion over than 10%.

### 2.2.3 Indium oxide-based catalysts

In<sub>2</sub>O<sub>3</sub> nanoparticles were produced which showed a 100% selectivity to methanol although conducted at high temperatures (300°C) [70]. This high selectivity and stability was attributed to the mechanism proposed by Ye *et al.* [71] occurring on oxygen defecting sites on In<sub>2</sub>O<sub>3</sub> surface, which could stabilize the reaction intermediates in the HCOO pathway as demonstrated in Figure 2.7. Gao *et al.* [72, 73] constructed a bi-functional catalytic system using In<sub>2</sub>O<sub>3</sub> combined with ZSM-5 (zeolites) and SAPO-34, where high methanol selectivity (80%) and low CO selectivity (<50%) from direct CO<sub>2</sub> hydrogenation path. In<sub>2</sub>O<sub>3</sub> rises as a highly effective catalyst for the synthesis of methanol through direct CO<sub>2</sub> hydrogenation [18]. This suggests that In could be a good promoter for several catalytic systems for CO<sub>2</sub> hydrogenation to methanol.

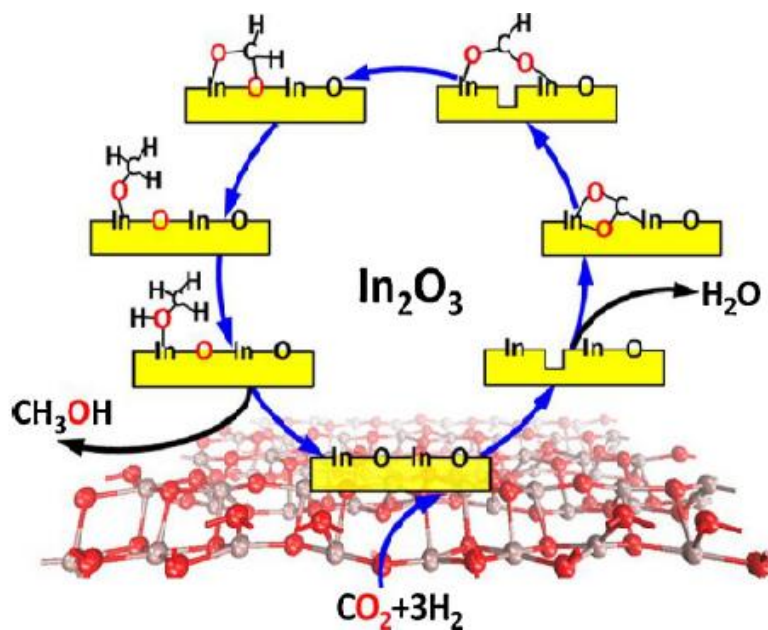


Figure 2.7. Mechanism of active oxygen sites on  $\text{In}_2\text{O}_3(110)$  surface [71]

The work of Ye *et al.* [21] demonstrated the improved catalytic performance after addition of Pd to obtain  $\text{Pd}_4/\text{In}_2\text{O}_3$  catalyst, since  $\text{H}_2$  breakdown adsorption sites were improved by the presence of Pd. In addition,  $\text{Pd}/\text{In}_2\text{O}_3$  was introduced by Rui *et al.* [20], where the preparation method consisted of mixing the  $\text{In}_2\text{O}_3$  (powder) with a Pd peptide composition as demonstrated in Figure 2.8. Results exhibit high methanol selectivity over 70% and activity of 20%.

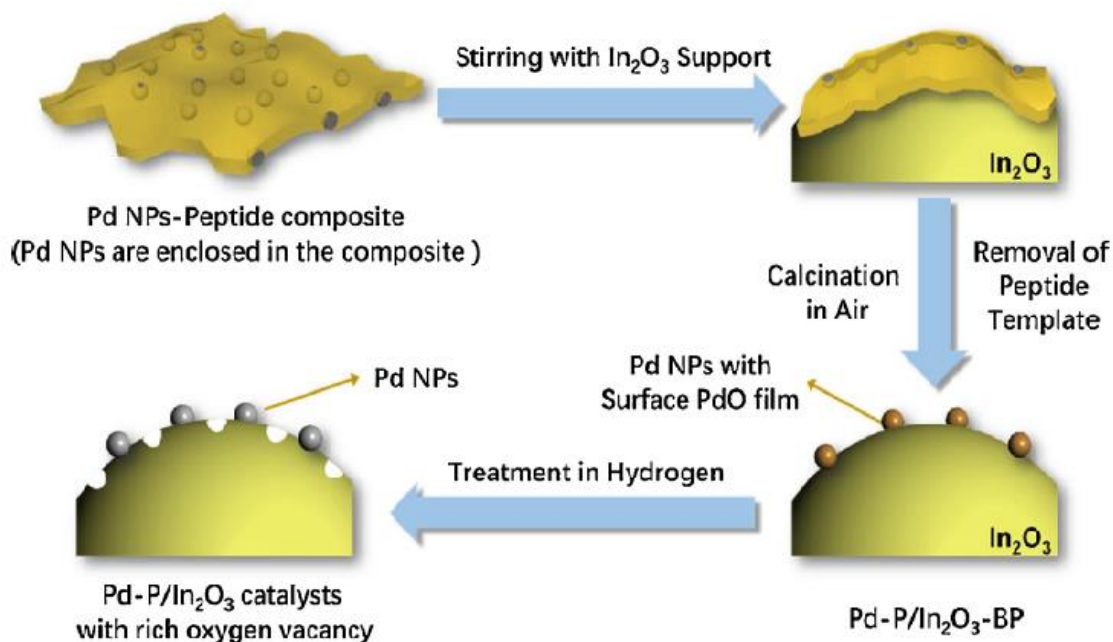


Figure 2.8. Preparation method of  $\text{Pd}/\text{In}_2\text{O}_3$  catalyst using Pd peptide composition and  $\text{In}_2\text{O}_3$  powder [20]

### 2.3 Other catalytic systems for CO<sub>2</sub> hydrogenation to methanol

The use of palladium (Pd) was demonstrated by several studies. CO<sub>2</sub> hydrogenation on Pd/ZnO catalysts was conducted in comparison between different catalyst preparation methods [74]. The catalyst showed a decrease in CO production through RWGS reaction. In addition to that, a high active surface area of Pd-Zn alloy was found which was responsible for the increased methanol selectivity. Bahruji *et al.* [75] conducted a study on a Pd/Zn catalyst supported with TiO to further improve catalyst performance. Another study found that the use of carbon nanofibers (CNFs) as support for Pd/ZnO catalysts improved the performance compared to the conventional Pd/ZnO catalyst. This was attributed to the small particle size (60.8 nm) of CNF supported Pd/ZnO that enhanced methanol selectivity [76]. A further study suggested that a trimetallic catalyst of PdCuZn/SiC (SiC = silica carbide) could be a viable methanol synthesis catalysts, as CO formation was inhibited [77].

Hartadi *et al.* [78] examined CO<sub>2</sub> hydrogenation to methanol over an Au/ZnO catalyst. They found that the catalyst showed comparable metal mass-normalized activity but was more selective for methanol than Cu/ZnO/Al<sub>2</sub>O<sub>3</sub>. In contrast to the beneficial effect of CO on methanol synthesis on Cu/ZnO/Al<sub>2</sub>O<sub>3</sub>, it was found that the addition of CO decreased the methanol formation rate on the Au/ZnO catalyst. Therefore, it was proposed that the hydrogenation of CO<sub>2</sub> and CO to methanol proceeded via different, independent pathways.

A study on a Ga<sub>2</sub>O<sub>3</sub> supported Pd catalyst found that the Pd-Ga interface formed an active site for methanol formation. The high activity of the catalyst was attributed to high metal dispersion and strong electron transfer between Pd and Ga, which was proposed to facilitate the activation and hydrogenation of reaction intermediate [79].

Methanol synthesis from H<sub>2</sub>/CO<sub>2</sub> over different metals supported on Mo<sub>6</sub>S<sub>8</sub> (M= K, Co, Ti, Rh, Ni, and Cu) was reported by Liu and Liu [80]. Methanol was produced using a modified model Mo<sub>6</sub>S<sub>8</sub> catalyst concluded from the DFT calculations. The outcome of this report showed that Mo<sub>6</sub>S<sub>8</sub> behavior changed significantly due to different modifiers used, where potassium (K) was the most promising for methanol synthesis. Chen *et al.* conducted experiments on Cu and Pd supported on Mo<sub>2</sub>C. They found that methanol production was enhanced compared to Mo<sub>2</sub>C and that the catalyst showed promising stability [81].

Sharafutdinov *et al.*[82] presented an intermetallic Ni-Ga catalyst, which showed that the intermediate phase of Ni<sub>5</sub>Ga<sub>3</sub> was a good inhibitor for methane generation and promoted



methanol selectivity. Studt *et al.*[83] also conducted a similar study, where successful CO<sub>2</sub> hydrogenation was done on Ni<sub>2</sub>Ga<sub>3</sub> active sites, which exhibited high methanol selectivity.

The use of In has been reported to have higher stability and selectivity compared to the benchmark Cu/ZnO/Al<sub>2</sub>O<sub>3</sub> catalyst for methanol synthesis from CO<sub>2</sub>. A low pressure methanol synthesis catalyst comprised of Ni<sub>a</sub>In<sub>b</sub>Al/SiO<sub>2</sub> (a=0-8.3, b=0-9.1) was developed, which showed high activity compared to the commercial catalyst at atmospheric pressure [84]. A bimetallic Pd-In catalyst was proposed by Garcia-Trenco *et al.* [85], where the most optimum Pd/In catalyst consisted of 8 nm nanoparticles covering an In enriched surface in a Pd/In intermetallic phase, of which it achieved a methanol selectivity higher than 80%. Table 2.2 summarizes the catalysts mentioned in section 2.3 .

Table 2.2. Summary of selected catalysts

Catalysts	Temperature (C°)	Pressure (Bar)	H <sub>2</sub> /CO <sub>2</sub> molar ratio	CO <sub>2</sub> conversion (%)	CH <sub>3</sub> OH selectivity (%)	Ref.
Pd/ZnO	250	20	3/1	11.1	59.0	[74]
PdZnO/TiO <sub>2</sub>	250	20	3/1	10.1	40.0	[75]
PdZnO/CNFs	275	10	9/1	3.29	12.1	[76]
PdCuZnO/SiC	200	10	9/1	–	80.9	[77]
Au/ZnO	240	50	3/1	0.4	49.0	[78]
Au/ZnO	240	50	3/1	1.0	70.0	[78]
Pd/plate Ga <sub>2</sub> O <sub>3</sub>	250	50	3/1	17.3	51.6	[79]
Pd/Mo <sub>2</sub> C	135	–	3/1	–	95.0	[81]
NiGa/SiO <sub>2</sub>	250	10	3/1	–	98.3	[82]
Ni <sub>3.5</sub> In <sub>5.3</sub> Al/SiO <sub>2</sub>	260	10	3/1	30.8	2.3	[84]
Pd/In	190	50	3/1	–	94.0	[85]

## 2.4 Catalyst synthesis

Different techniques of HT synthesis are present such as precipitation at constant pH, deposition/precipitation reactions, hydrothermal synthesis etc., however it has been shown that precipitation at constant pH, also known as coprecipitation, is a promising method for preparing highly active and stable catalysts [86]. Various parameters are taken into consideration to produce pure HTs, where the total cationic concentration is determined to be 0.5 M to ensure the formation of an HT structure.

### 2.4.1 Catalyst synthesis by co-precipitation

#### 2.4.1.1 Hydrotalcite or layered double hydroxides

The primary active sites for methanol synthesis on a commercial catalyst are widely recognized as copper [87]. Through literature studies the best performing catalytic systems were the ones having the best dispersion between the metallic copper and the Zn or/and Al<sub>2</sub>O<sub>3</sub> [88]. An easy manner to obtain such high dispersion is using precursors containing Cu, Zn, Al with a HT structure [89]. HT-like materials, which are also referred to as lamellar double hydroxides (LDH), are an example of the lamellar solids which have lamellae consisting of positive charges where they are balanced with interchangeable anions present in the interlayer region [17].

LDH structure has an approximate composition of Mg<sub>6</sub>Fe<sub>2</sub>(OH)<sub>16</sub>CO<sub>3</sub>.H<sub>2</sub>O where Mg's octahedral structure forms infinite sheets of which they are stacked on top of each other and connected through hydrogen bonds [90]. Mg and Fe can be changed with a compound having the same ionic charge where 2+ and 3+ are for Mg and Fe respectively. Mg can be replaced by components such as Cu<sup>2+</sup>, Ni<sup>2+</sup>, Zn<sup>2+</sup>, etc. while Fe can be replaced by Al<sup>3+</sup>, In<sup>3+</sup>, etc.

According to Zhang *et al.* HT-like components have a general formula of [M<sup>2+</sup><sub>1-x</sub>M<sup>3+</sup><sub>x</sub>(OH)<sub>2</sub>]<sup>x+</sup>(A<sup>n-</sup>)<sub>x/n</sub>.mH<sub>2</sub>O, where M<sup>2+</sup> and M<sup>3+</sup> present the divalent and trivalent metal cation respectively [91]. Usually, the charge composition is achieved by the interaction between the brucitic layers as shown in Figure 2.9 [40]. In the brucitic layer, water molecules are found in the inner layers of which they settle into the vacant sites and bond the hydroxyl groups of the brucitic layers via hydrogen bonds [40]. Through a controlled thermal decomposition of HT compounds the mentioned oxides can be obtained [92]. Many studies concluded that having a high Cu dispersion with the right amount and strength of adsorption favor the hydrogenation of CO<sub>2</sub> [93-95]. In addition to that, it was proven that HT components have a high resistance against stability, homogenous dispersion of M<sup>2+</sup> and M<sup>3+</sup>, larger surface area, and better basic properties which presents HTs as a promising area for development [96-98].

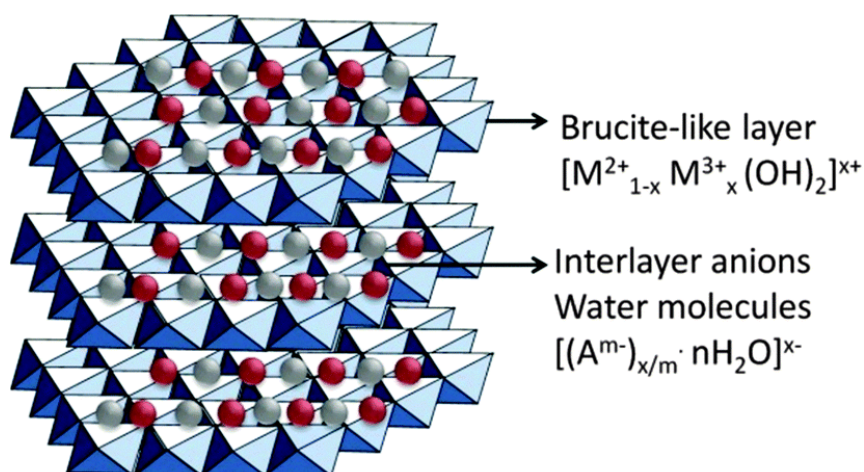


Figure 2.9. Schematic illustration of layered double hydroxide structure and chemical components [99].

The nature of  $M^{2+}$  and  $M^{3+}$  can be altered to fit in the pores of the packed pattern of the hydroxyl groups in the brucitic layer. In this study, Cu and Zn bimetallic alloys were introduced as the basis for the methanol synthesis catalyst. The variant behavior of the  $Cu^{2+}$  ion was attributed to the actual nature of the Cu itself which forms compounds interpreted by the Jahn-Teller effect where the distortion in the octahedral structure provides an energy gain [39]. Various studies have shown that Cu and Zn can be applied as a substitute for the Mg due to the close ionic radius of Mg (0.072 nm) as shown in Table 2.3 [90]. In addition, the radius of In was added to show the large ionic radius it has compared to Al which demonstrates a detectible change in the catalyst's performance.

Table 2.3. Ionic radii of cations [90]

$M^{2+}$	Radius (nm)	$M^{3+}$	Radius (nm)
Cu	0.069	Al	0.05
Zn	0.074	In	0.081

#### 2.4.1.2 Coprecipitation method

Considering different preparation methods and procedures the main applied method is coprecipitation. The different molecular ratios and work conditions can affect the catalyst's performance [100]. The synthesis of HT components can be summed up by the nucleation and growth of the metal hydroxide layer due to the mixing of an aqueous solution where two metallic salts are used to obtain a base and an anion [101]. The usage of this synthesis technique is accompanied by restricting condition where the preferred interlayer anion is held as toughly

as the counterion in the metal salts. Thus, metal nitrates and metal chlorides are extensively used [102].

The method of synthesis in this report is co-precipitation at low supersaturation. This method is carried out at low constant temperature between pH 7 and pH 10 to insure the formation of HT structures [103]. Afterwards aging is applied, and then drying at a temperature of maximum 120°C.

#### **2.4.2 Aging**

Aging is a post preparation process of which the aqueous mixture is preserved at either standard temperature or under constant heat where stirring is applied in the ongoing process. This process contributes in the formation of crystallites of a large size by enhancing the LDH structure [104]. It is of great importance to mention that the temperature of aging affects the crystalline growth that alters the catalyst's efficiency later in its practical application. When the aging process is done at temperatures till 90°C, improved hexagonal structure will be formed due to eased ion diffusion which will result in larger size crystals with more stable energetic structure [105].

#### **2.4.3 Calcination**

Calcination is the thermo-chemical treatment of aged precursors where they are heated in the presence of oxygen or synthetic air at a constant temperature. Calcination will change the composition from hydroxide to mixed oxides. The temperature of the calcination must be taken into consideration, since it must be high enough to ease the formation of metal oxides, however low enough to avoid sintering phenomena that will decrease surface area of the catalyst.

#### **2.4.4 Reduction**

Reduction is considered as an activation phase for catalytic reactions. Catalysts are activated using a reducing agent (most commonly hydrogen) which transforms metal oxides to active metal species. The main parameter in the reduction process is the temperature applied, which can affect metal surface area and dispersion.

### **2.5 Catalyst characterization**

#### **2.5.1 X-ray diffraction (XRD)**

X-ray diffraction method gives insights concerning the crystalline materials. Intensities of different peaks, which are later compared and evaluated to an existing database of materials, are used to identify the structure and content of the tested sample, to determine the nature of the existing phases [106]. The characterization process is done by directing x-ray to the atom,

which creates a reflection of different waves depending on the structures available in the sample. Bragg's law equation (eq.2.1) explains the relationship between the wavelength  $\lambda$ , the spacing between crystal lattice planes of atoms  $d$ , and angle of occurrence  $\theta$  [107].

$$\lambda = 2 \times d \times \sin\theta \quad (2.1)$$

At the same time,  $d$  can be calculated by the Scherrer equation (eq. 2.2) [108].

$$d = \frac{K \lambda}{B \cos \theta} \quad (2.2)$$

Where  $B$  presents the total width at XRD's half maximum peak (radians) and  $K$  is a numerical factor denoted to the crystallite-shape factor.

The x-rays in this process are formed by a cathode ray tube with a beam of electron radiating toward a metallic object. The intensity of the diffraction as a function of angle is documented. Three main diffraction techniques exist and the powder technique (PXRD) is the most common one which uses a stable wavelength. All the diffraction of the lattice can be acquired due to the random placement by analyzing the sample through a  $2\theta$  angles.

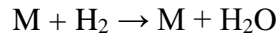
There are various gains and applications of PXRD including study of polymorph, different temperature and phase transition, etc. [109]. Using PXRD, the location of the diffraction patterns provides insights concerning the size and shape of the composition, while on the other hand the intensities are used to observe the atom's position of the sample. By comparing the XRD peak positions with a database, the sample's composition can be defined. Geometry of the lattice is indicated by the peaks considering dimensions and internal symmetry.

In addition to that, atom's arrangement and crystalline size can be observed by considering the intensities of the beams. Various elements can affect the intensity, for instance the adding of atoms, the quantity of crystal oriented in the Bragg's angle, and the affinity to atom's order [107].

### **2.5.2 Temperature programmed reduction**

Temperature Programmed Reduction (TPR) is a manner by which metal oxides, mixed metal oxides, and metal oxides distributed on a support are identified. A TPR outline offers a qualitative description of the oxidation state of reducible species such as quantity of reducible species, and the temperature at which the reduction is taking place. Throughout TPR, a reducing gas mixture (mainly formed of hydrogen) is introduced over the mixed oxide (MO) while the temperature is increasing linearly with time. The reaction between reducing gas and

MO will lead to the formation of a metal (M) and water, whereas concentration of hydrogen decreases. [101].



The thermal conductivity (TC) is measured by a thermal conductivity detector, which shows a decrease in TC of the gas flow. Nitrogen or argon are typically chosen as carrier gases. In addition, the concentration of hydrogen must range between 1-10% in order to maintain a high detector measurement, since the variation of TC is proportional to the mole fraction at a low concentration of reactant gas in the carrier gas mixture. In addition, TPR can also study the coke deposition on catalysts [110].

The results obtained from TPR can differ depending on the heat rate, concentration of hydrogen in the carrier gas, and the flow rate of the carrier gas. The criteria of analysis were suggested as the following:  $S^{\circ}(V \times C^{\circ}) = 55-14$  (s) and  $\beta \times S^{\circ}/(V \times C^{\circ}) < 2$ . The heating rate is  $\beta$  ( $^{\circ}C/min$ ), the amount of reducible species initially is  $S^{\circ}$  ( $\mu mol$ ), whereas total flowrate is represented by  $V$  ( $cm^3/min$ ), and the initial concentration of reducing gas is  $C^{\circ}$  ( $\mu mol/cm^3$ ) [111].

### 2.5.3 Nitrogen adsorption-desorption

Gas adsorption-desorption measures the surface area and characterizes the pore size of porous material. Two types of adsorption are available: physisorption and chemisorption which differentiate according to the power of interaction. The most appropriate one is physical adsorption since it is conducted at low heat of adsorption that doesn't affect or disturbs the structure of the surface during measurement, whereas in chemical adsorption multiple layers of adsorbate cover the surface during measurement. Furthermore, there is no activation energy, thus the equilibrium will be reached rapidly. Adsorption and desorption harnessed data contribute in characterizing pore volume, pore size, and pore distribution [112].

The commonly applied theory to conclude surface area of porous material is the Brunauer-Emmett- Teller (BET). This theory considered the multi-layer adsorption which resulted with the following BET equation (eq. 2.3).

$$\frac{1}{W \left( \frac{P}{P_0} - 1 \right)} = \frac{1}{W_m C} + \frac{C - 1}{W_m C} \left( \frac{P}{P_0} \right) \quad (2.3)$$

Where  $P$  and  $P_0$  are the equilibrium and the saturation pressure of adsorbates at the adsorption temperature,  $C$  represents BET constant affiliated to the adsorbate and adsorbent interactions.  $W_m$  can be determined through the collection and plot of a graph of  $1/[W \times (P/P_0 - 1)]$  versus

$P/P_0$ , using the measurement data of the accumulated gas quantity adsorbed versus gas pressure at a specific temperature. The International Union of Pure and Applied Chemistry (IUPAC) classifies sorption isotherms into six types from I till VI which are demonstrated in Figure 2.10 [113].

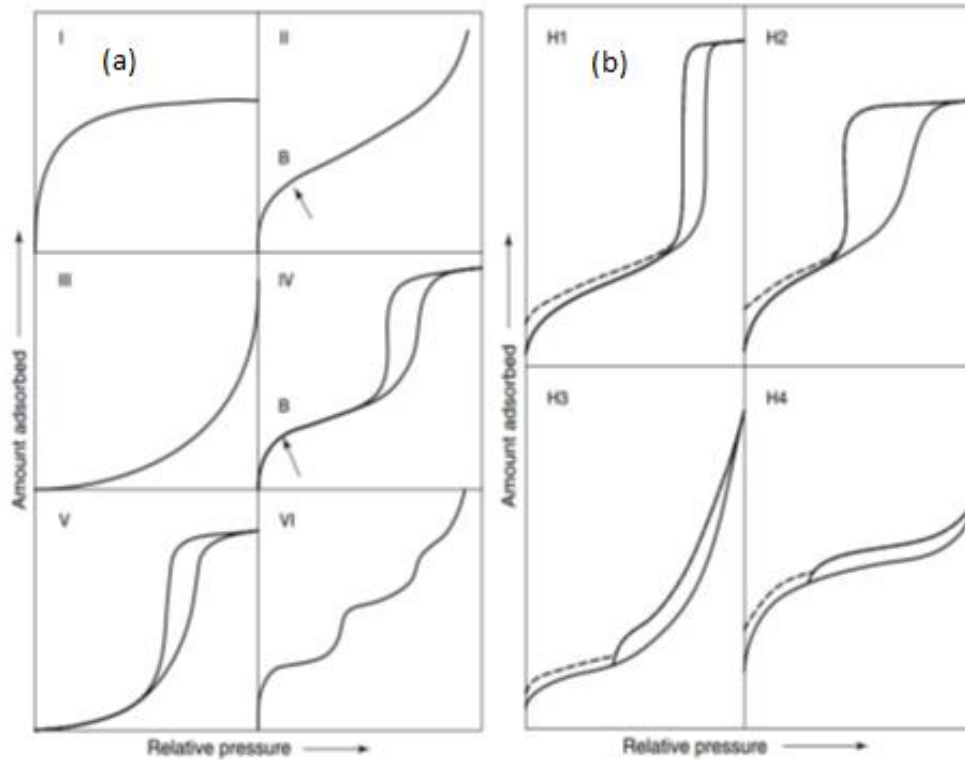


Figure 2.10. (a) Types of physisorption isotherms (b) Types of hysteresis loops [113]

The BET theory is perceived as simple and can be affiliated with the isotherm types. The BET theory also shares with the experimental isotherms a common approach to the relative pressure near the completed monolayer, thus making the BET theory the best method to measure surface area.

The pore volume and pore size distribution are measured using the Barrett-Joyner-Halenda (BJH) method. During measurement, the data is computed using the gas desorption isotherm and adjusted Kelvin equation. Eventually the correlation between the volume of capillary condensate and relative pressure is defined by a relation between capillary radius and vapor pressure depression [114].

#### 2.5.4 Gas chromatography

Gas Chromatography (GC) is a widely used measurement method to separate and determine the composition of volatile compounds. GC measurement method is fast, simple, and capable

of measuring a variety of organic and inorganic compounds. Throughout the process, the sample is initially vaporized and carried by a fluidized gas (carrier gas) to the chromatographic column. The vapor pressure of each component is relative to the column's temperature and the component's affinity with the stationary phase. The components keep on shifting from mobile gas phase to the stationary phase due to the difference in vapor pressure. Once the component is in the mobile gas phase, it is instantly carried to the detector [115]. Full isolation (leak free) of the system is crucial to prevent any characterization failure, this can be achieved by using a metal or glass tube as a column.

The data is analytically quantified based on the chromatogram readings, peaks are measured, and calculations are performed relative in the desired units. Quantitative analysis is divided into five different methods which are area normalization, area normalization with response factors, standard addition, internal standard, and external standard [116]. The most common method used for gas analysis is external standard.

## **2.6 Kinetics of methanol synthesis**

Carbon dioxide hydrogenation reaction is by far the most preferred reaction, which happens in parallel with the reverse water shift reaction [117]. Various kinetic models were proposed in literature, each considering different thermodynamic and kinetic parameters, different feed composition and catalytic systems used. Some of these models studied the synthesis of methanol from CO<sub>2</sub> and some considered synthesis from an H<sub>2</sub>/CO feed. Different kinetic laws were derived, and they were based on the rate determining step concluded from the reaction's mechanism.

### **2.6.1 Kinetic models**

A kinetic model was established by Van den Bussche and Froment [118] which took into consideration only the carbon dioxide hydrogenation and the water shift (WGS) reaction. In this model they assumed CO<sub>2</sub>, from WGS, is the main carbon source in this reaction. The rate determining step was the dissociative adsorption of CO<sub>2</sub> and H<sub>2</sub>.

Park et al. suggested a kinetic model which was based on the Langmuir-Hinshelwood-Hougen-Watson (LHHW) mechanism that considers all the three reactions [(1) (2) (3)][119].

Another kinetic model based on the Power Law was established by Askgaard *et al.*[120] and Kobel *et al.* [121]. Power Law model considers that the thermodynamic equilibrium is obtained by 16 elementary steps. This model considers the comparison between experimental data, and



the modeled data. Through the Power Law, different parameters can be adjusted in order to narrow down the difference between experimental and modeled data.

Various microkinetic studies have been performed of which only two main studies will be mentioned in this section. Grabow and Mavrikakis [122] suggested a micro kinetic model over the commercial catalyst Cu/ZnO/Al<sub>2</sub>O<sub>3</sub> based on 49 elementary steps which demonstrated different reaction intermediates involved in methanol synthesis. The results from this model showed that almost 75% of the methanol was obtained from CO<sub>2</sub> hydrogenation.

Another study by Kunkes *et al.* [123] tackled a very important question towards the reaction's mechanism which whether methanol synthesis and RWGS have a parallel pathway, or have some intermediates in common, or methanol synthesis precedes RWGS and CO hydrogenation. Tests performed on Cu/MgO, Cu/SiO<sub>2</sub>, and Pd/SiO<sub>2</sub> showed that the 2 reactions have no common intermediates. On the other hand, tests performed on Cu/ZnO/Al<sub>2</sub>O<sub>3</sub> showed that CO<sub>2</sub> hydrogenation doesn't go through either RWGS or CO hydrogenation. Thus given the fact that RWGS reaction and methanol synthesis have separate pathways, Cu/ZnO/Al<sub>2</sub>O<sub>3</sub> rises as a promising catalyst for further development and modification [123].

Various studies concerning macrokinetics were performed by Graaf *et al.* [124-126] where they established a kinetic model based on the LHHW mechanism that considered all the 3 reactions [(1) (2) (3)] conducted over a Cu/ZnO/Al<sub>2</sub>O<sub>3</sub> Haldor Topsoe catalyst. These studies considered the rate determining steps according to the dual site LH mechanism. These studies were considered as the basis for recent kinetic models' construction.

### **2.6.2 Power Law model**

The Power Law model is considered as a simple model and can be used in any kinetic reaction analysis since kinetic analysis can be done even though little knowledge about the reaction's mechanism is available [127]. Several models has been suggested by different studies [128, 129] with no defined mechanism of which they can only be used within a specified range of temperatures, conversion, and partial pressures.

The Power Law model works by executing theoretical and experimental analysis of the chemical reaction and comparing the data together. Eventually this serves the purpose of narrowing down the divergence between theoretical and experimental analysis. This model is used to anticipate certain changes in mechanism that might occur during the reaction, and gather quantitative data about reaction rates, which will help in the advancement of the catalytic process.

Power Law model is implemented using a series of equations that cover thermodynamics, activation energy, and catalytic activity. This model was based on several assumptions where two reactions were considered: (i) CO<sub>2</sub> hydrogenation to methanol (j= methanol); (ii) reverse water gas shift reaction (j= CO). Equations and formulas mentioned are extracted from the work of Kobl *et al.* [121] and the quantitative interpretation of Graaf *et al.* [124-126] with certain modifications performed to suite an H<sub>2</sub>/CO<sub>2</sub> feed . As mentioned, this model was divided into two sections: Theoretical and experimental. The following equations give a representation of this model:

### **Theoretical Approach:**

The thermodynamic equilibrium is referred to as  $\beta_j$  where  $j$  is the reaction index. The equilibrium was added to the kinetic equations to consider the reverse reactions occurring.  $\beta_j$  representation was the following:

$$\beta_{methanol} = \frac{P_{(methanol,out)} \times P_{(H_2O,out)}}{K_{methanol} \times P_{(methanol,out)}^3 \times P_{(CO_2,out)}} \quad (2.4)$$

$$\beta_{CO} = \frac{P_{(CO,out)} \times P_{(H_2O,out)}}{K_{CO} \times P_{(H_2,out)} \times P_{(CO_2,out)}} \quad (2.5)$$

Where  $K_j$  represents the equilibrium constant.

On the other hand,  $K_j$  was presented based on the following interpretation from Graaf *et al.*'s work [125], it should be noted that their work was based on a H<sub>2</sub>/CO feed but modifications were performed to suite the H<sub>2</sub>/CO<sub>2</sub> feed:

$$K_{methanol} = (K_{\phi_{methanol}} \times K_{P_{methanol}}) * K_{CO} \quad (2.6)$$

$$K_{CO} = K_{\phi_{CO}} \times K_{PCO} \quad (2.7)$$

Where  $K_p$  and  $K_{\phi}$  present the partial pressure coefficient and the fugacity coefficient respectively. They represent as the following:

$$K_{P_{methanol}} = \frac{Y_{methanol}}{Y_{CO} \cdot Y_{H_2}^2} \quad (2.8)$$

$$K_{PCO} = \frac{Y_{H_2O} Y_{CO}}{Y_{CO_2} \cdot Y_{H_2}} \quad (2.9)$$

Where  $Y$  is the mole fraction of components. And since the chemical reaction in this study was occurring in non-ideal gas conditions where the reaction is occurring at 30 bars, hence the fugacity correlation is relatively small and might be neglected [130]. Thus,  $K\phi_{methanol} = K\phi_{CO} \approx 1$ .

This model is temperature sensitive, thus the use of activation energy factor  $Ea$  and a pre-exponential factor  $k$  is essential to cover this matter. Furthermore, based on Hu *et al.* [131] any appearance of dew point temperatures is not anticipated since the reaction's pressure is not exceeding 100 bar. Thus, based on these assumptions turnover frequency (TOF) equations were formed into a power law expression as the following:

$$TOF_{methanol} = k_{methanol} \exp\left(\frac{-Ea_{methanol}}{RT}\right) P_{H_2}^{n_{methanol}} P_{CO_2}^{m_{methanol}} (1 - \beta_{methanol}) \quad (2.10)$$

$$TOF_{CO} = k_{CO} \exp\left(\frac{-Ea_{CO}}{RT}\right) P_{H_2}^{n_{CO}} P_{CO_2}^{m_{CO}} (1 - \beta_{CO}) \quad (2.11)$$

Where  $n_j$  and  $m_j$  are calculated with respect to the inlet pressure of  $H_2$  and  $CO_2$  respectively.

### **Experimental approach:**

The experimental approach is based on the following with the same index factors used in the theoretical approach:

$$n_j = \int_0^{t_R} F_j dt \quad (2.12)$$

Where  $n_j$  is the amount of component consumed over the entire experimental period,  $F_j$  is the molar flow rate, and  $t_R$  is the duration of the experiment.

Conversion of substances should be averaged over the experimental period and the selectivity can be determined based on the product's carbon-content. They are covered by the following equations:

$$X_{CO_2} = \frac{n_{CH_3OH} + n_{CO}}{n_{CO_2,in}} \times 100 \quad (2.13)$$

$$X_{H_2} = \frac{2n_{CH_3OH} + n_{H_2O}}{n_{H_2,in}} \times 100 \quad (2.14)$$

$$S_{CH_3OH} = \frac{n_{CH_3OH}}{n_{CH_3OH} + n_{CO}} \times 100 \quad (2.15)$$

$$S_{CO} = 1 - S_{CH_3OH} \quad (2.16)$$

The TOF values are calculated considering an equally active total surface area and both reactions happening on the Cu surface. TOF equations express as the following:

$$TOF_{CH_3OH} = \frac{n_{CH_3OH} \times N_A}{m_{cat} \times S_{Cu} \times N_s \times t} \quad (2.17)$$

$$TOF_{CO} = \frac{n_{CO} \times N_A}{m_{cat} \times S_{Cu} \times N_s \times t} \quad (2.18)$$

Where  $n$  is the number of moles of methanol,  $m_{cat}$  is the mass of the catalyst,  $S_{Cu}$  is the specific copper area,  $N_A$  is Avogadro's number,  $N_s$  is the number of surface copper atoms per unite surface area and  $t$  is the reaction time. In literature, the common used  $N_s$  value is  $1.46 \times 10^{19} \text{ m}^{-2}$  since planes of (100), (110), and (111) are assumed equal when exposed at Cu's surface [132].

Eventually, the theoretical TOF values are plotted versus the experimental TOF values to give a similar representation as the one in Figure 2.11. These plots are called parity plots where the quantitative comparison between theoretical and experimental data is performed. This comparison is essential to establish an understanding concerning how the mechanism works, and the validity of considered assumptions.

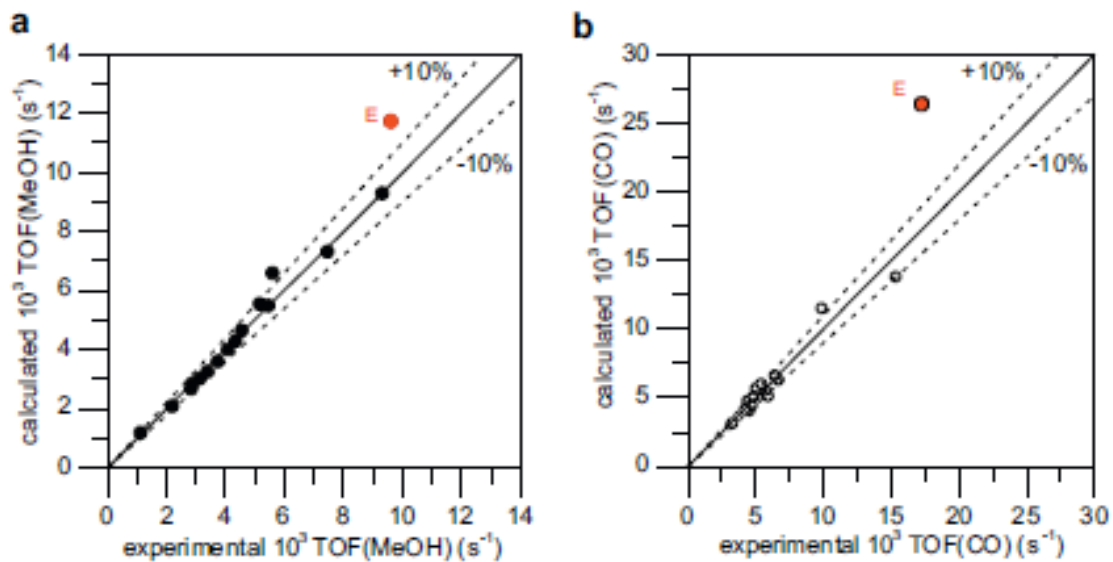


Figure 2.11. Example of parity plot representation of methanol synthesis (a) and Reverse Water Gas Shift Reaction (b) [121]

### 3 Experimental

#### 3.1 Materials and equipment

No further purification or modification was performed on the chemicals used throughout this report. A detailed summary of the chemicals used for catalyst preparation and gases for catalytic testing are summarized in Table 3.1.

Table 3.1. List of used chemicals for catalyst preparation and gases for activity tests.

No.	Materials	Chemical Formula	Manufacturer	Molecular Weight (g/mol)	Purity
1	Copper (II) Nitrate Trihydrate	Cu (NO <sub>3</sub> ) <sub>2</sub> ·3H <sub>2</sub> O	ACROS ORGANICS	241.59	≥ 99%
2	Zinc Nitrate hexahydrate	Zn (NO <sub>3</sub> ) <sub>2</sub> ·6H <sub>2</sub> O	Alfa Aesar	297.49	≥ 99%
3	Indium (III) Nitrate Hydrate	In (NO <sub>3</sub> ) <sub>3</sub> ·xH <sub>2</sub> O	EMSURE	318.83	≥ 99%
4	Aluminum Nitrate Nonahydrate	Al (NO <sub>3</sub> ) <sub>3</sub> ·9H <sub>2</sub> O	EMSURE	375.13	≥ 98.5%
5	Sodium Hydroxide	NaOH	EMSURE	40.0	≥ 99.2%
6	Sodium Carbonate	Na <sub>2</sub> CO <sub>3</sub>	EMSURE	105.99	≥ 99.9%
7	Silicon Carbide	SiC	Alfa Aesar	40.1	≥98.8%
8	Carbon dioxide	CO <sub>2</sub>	Yara Praxair	44	99.999%
9	Hydrogen	H <sub>2</sub>	Yara Praxair	2	99.999%
1	Nitrogen	N <sub>2</sub>	Yara Praxair	28	99.999%

#### 3.2 Catalyst synthesis

Throughout this study, the catalysts were synthesized using the conventional co-precipitation method. The precursors containing Cu, Zn, and Al are labeled as *X*-CuZnAl where *X* is the molar ratio of Cu and Zn in the reduced catalysts. Meanwhile the catalysts containing In was denoted as *X*-CuZnAl-*Y*-In where *Y* represents the weight percent of In in the catalyst. In this study, different molar ratios of the Cu-based catalyst were synthesized and tested, of which the best molar ratio was chosen to be synthesized with the addition of the different fractions of the In promoter. Table 3.2 below demonstrates all the catalysts synthesized with their compositions.

Table 3.2. Labels and characteristics of the prepared catalysts

Catalyst	Cu/Zn molar ratio	Catalyst composition (wt%)
1.5-CuZnAl	1.5	45 Cu – 3 Zn – 25 Al
1-CuZnAl	1	37.5 Cu – 37.5 Zn – 25 Al
0.5-CuZnAl	0.5	25 Cu – 5 Zn – 25 Al
1-CuZnAl-2.5-In	1	37.5 Cu – 37.5 Zn – 22.5 Al – 2.5 In
1-CuZnAl-5-In	1	37.5 Cu – 37.5 Zn – 20 Al – 5 In
1-CuZnAl-7.5-In	1	37.5 Cu – 37.5 Zn – 17.5 Al – 7.5 In

The HT synthesis method was concluded from a patent modified by Bhattacharyya et al. [103]. In this method co-precipitation at low super-saturation was adopted to produce catalysts from HT-like precursors. A specific stoichiometric amount of  $\text{Cu}(\text{NO}_3)_2 \cdot 3\text{H}_2\text{O}$ ,  $\text{Zn}(\text{NO}_3)_2 \cdot 6\text{H}_2\text{O}$ ,  $\text{Al}(\text{NO}_3)_3 \cdot 9\text{H}_2\text{O}$ , and  $\text{In}(\text{NO}_3)_3 \cdot x\text{H}_2\text{O}$  (for the promoted catalysts) were dissolved in an apparatus of deionized water (400 ml) to obtain a cation solution with a concentration of 0.5 M. Whereas, NaOH and  $\text{Na}_2\text{CO}_3$  were used to form the anion solution by dissolving adequate amounts into deionized water (400 ml). Using a graduated funnel, the cation solution was added dropwise to the anion solution, while stirring was applied at 700 RPM for almost 2 hours (1 drop/second) at room temperature. Afterwards, the pH of the mixture was adjusted to become closer to pH 9 using some droplets of nitric acid. The pH adjustment is of great importance, since according to Xiao *et al.* catalysts prepared at pH 9 have resulted in better HT structures and performed best [65]. The mixture was heated up to 85°C while stirring was applied (650 RPM) and a continuous flow of nitrogen was carried out for 18 hours. Then, vacuum filtering was applied, where the slurry mixture was washed several times with deionized water to obtain a neutral pH. The filter cake was dried in a 90°C oven overnight. The catalyst was then calcined using a quartz reactor unit at 500°C with a temperature increase rate of 5°C/min, for a duration of 5 hours.

### 3.3 Characterization of catalysts

#### 3.3.1 X-ray diffraction (XRD)

XRD studies of catalysts were performed for the fresh and calcined HT-like precursors catalysts using a Bruker-AXS Microdiffractometer D8 Advance which uses a  $\text{CuK}\alpha$  radiation source. These signal configurations were recorded with a  $2\Theta$  range of 10°-90°, with 1°/min step

increment. The structural properties were obtained by the Bragg's law equation (eq.2.1) and the Scherrer equation (eq.2.2) mention in section 2.5.1.

### **3.3.2 Temperature programmed reduction (TPR)**

TPR measurements were conducted using a Micromeritics Autochem II ASAP 2920 analyzer with a thermal conductivity detector (TCD). The calcined samples of about 70 mg were degassed at 200°C in He flows for a time of 20 minutes to eliminate any adsorbed H<sub>2</sub>O and CO<sub>2</sub>. After cooling to 50°C, the reducing gas mixture (10 vol% H<sub>2</sub> in argon) was passed over the samples with flow rate of 50 mL/min. The temperature was ramped up to 550°C at a rate of 10°C/min and held for 30 minutes.

### **3.3.3 Nitrogen adsorption – desorption**

Nitrogen adsorption-desorption measurements were obtained by using a Micromeritics TriStar 3000 instrument at -196°C with liquid nitrogen. Preceding the analysis, samples were degassed at 180°C under vacuum overnight.

## **3.4 Catalytic Activity Tests**

The unit used in this study was a fixed-bed tubular reactor as shown in Figure 3.1. The reactor is composed of a temperature resisting metal. The reactor was supplied with a gas feed of N<sub>2</sub>, H<sub>2</sub>, and CO<sub>2</sub> which were controlled by a mass flow control unit (Bronkhorst). The pressure regulator was set on 5 bars for each gas feed line. A pressure gauge and a back-pressure controller were placed to monitor and control the pressure inside the reactor. The reactor was heated up using an electrical oven regulated by a temperature regulator (Eurotherm 328). A thermocouple of type K was used within the reactor and placed below the catalytic bed.

Figure 3.1 shows a schematic representation of the experimental unit used in the catalyst activity tests and Table 3.3 shows the dimensions of the reactor. Prior to the activity tests, the catalysts went through a reduction procedure under a flow rate of 50 mL/min with 50 vol% H<sub>2</sub>/N<sub>2</sub> in a fixed bed tubular reactor at 350°C for 2 hours. The temperature was built up by a rate of 5°C/min to reach 350°C. After reduction the bed was flooded with N<sub>2</sub> for 30 minutes and the reactor was cooled to below 60°C. Subsequently, a H<sub>2</sub>/CO<sub>2</sub>/N<sub>2</sub> flow of 3/1/1 of 50 mL/min was used to purge the reactor for 15 min. Finally, the pressure inside the reactor was increased to 30 bars and then the temperature was increased to the desired reaction temperature. The CO<sub>2</sub> conversion and CH<sub>3</sub>OH selectivity were calculated according to the following formulas, where N<sub>2</sub> was used as internal standard to calculate the flowrates of each species. The CO<sub>2</sub> conversion and CH<sub>3</sub>OH selectivity was calculated by the following equations:

$$X_{CO_2} = \frac{n_{CO_2}^{in} - n_{CO_2}^{out}}{n_{CO_2}^{in}} \times 100\% \quad (3.1)$$

$$X_{CH_3OH} = \frac{n_{CH_3OH}^{out}}{n_{CO}^{out} + n_{CH_3OH}^{out}} \times 100\% \quad (3.2)$$

Where  $n_i^{in}$  and  $n_i^{out}$  represent the number of moles of each gas in the inlet and outlet of the reactor.

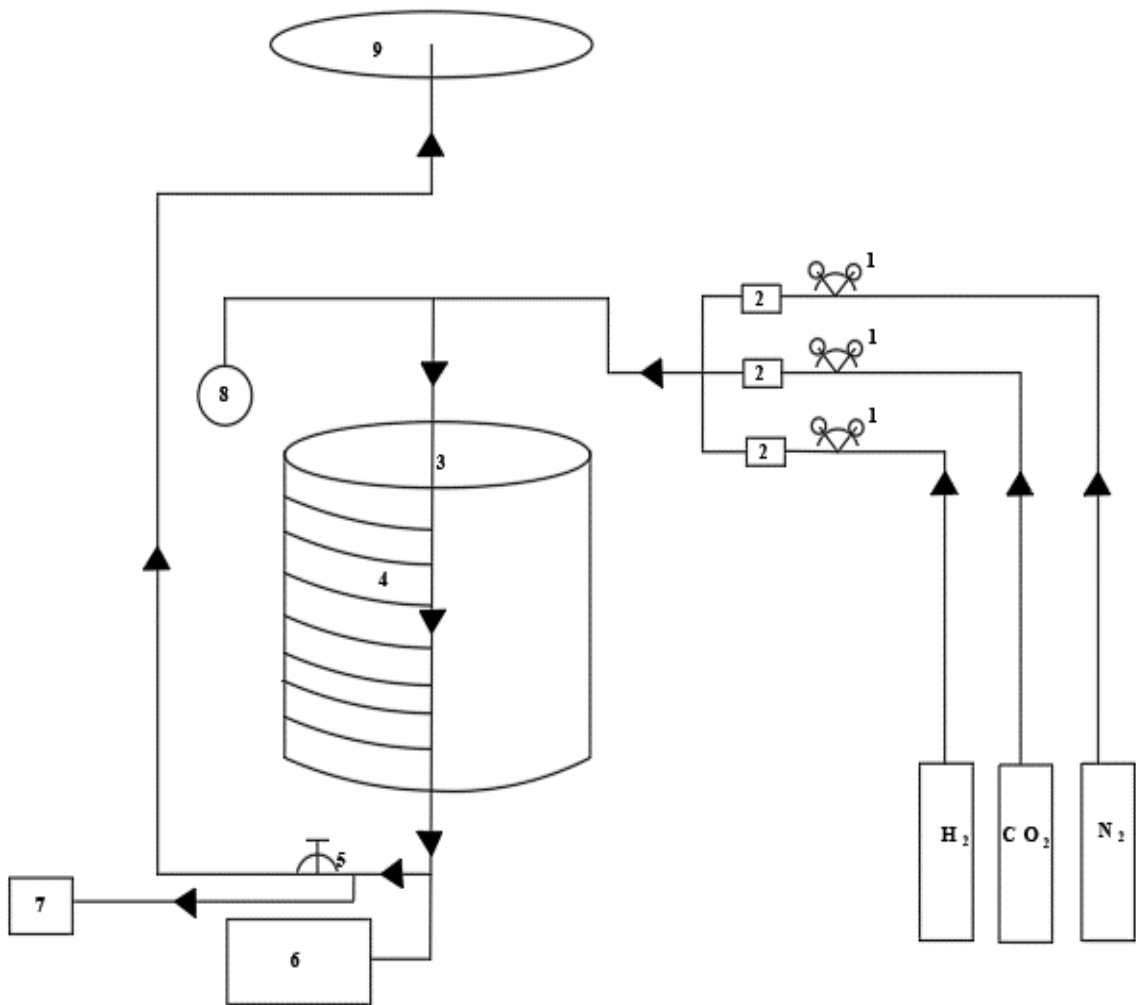


Figure 3.1. Schematic representation of the experimental set up

1: Pressure regulator with two pressure gauges, the one on the right gives the amount of gas in the gas bottle (bars), while the one on the left gives the regulated pressure value of the system.

2: Mass flow meter.

3: Reactor bed; detailed specs mentioned in Table 3.3.



- 4: Electric oven resistor's distribution within the reactor bed.
- 5: Back-pressure regulator.
- 6: Temperature controller.
- 7: Gas chromatography unit.
- 8: Pressure gauge indicating the pressure inside the reactor bed.
- 9: Gas exit vent.

Table 3.3. Specs of the reactor bed

Inner Diameter of Bed	6 cm
Outer Diameter of Reactor	14 cm
Vertical Length of Reactor	35 cm

## 4 Results and discussion

### 4.1 Characterization of catalysts

#### 4.1.1 XRD analysis of un-promoted catalysts

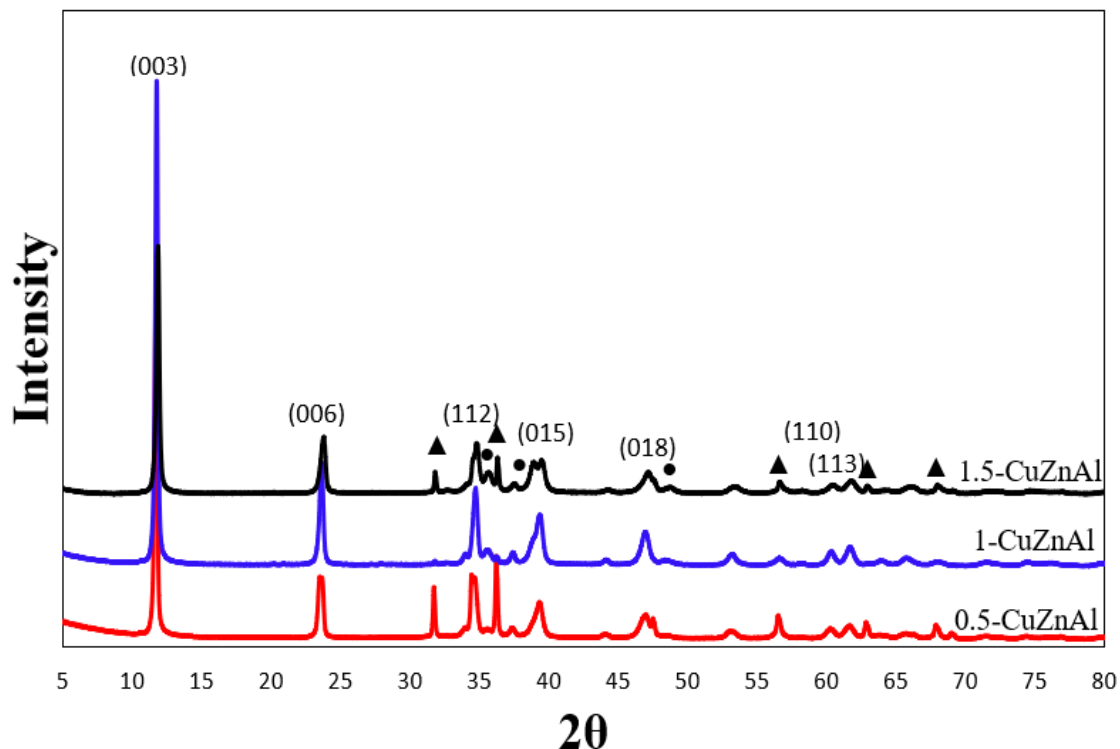


Figure 4.1. XRD patterns of un-promoted as-prepared catalysts, (▲) ZnO and (●) CuO

XRD patterns of the as-prepared, un-promoted catalyst precursors are presented in Figure 4.1. As expected, the diffractograms of the catalyst display typical HT-like structure as the major phase. The peaks at  $2\theta$  of  $11.78^\circ$ ,  $23.7^\circ$ ,  $34.7^\circ$ ,  $39.4^\circ$ ,  $47.1^\circ$ ,  $60.2^\circ$ , and  $61.6^\circ$  which refer to peaks (003), (006), (112), (015), (018), (110), and (113) were characteristics of  $\text{Cu}_3\text{Zn}_3\text{Al}_2(\text{OH})_{16}\text{CO}_3 \times \text{H}_2\text{O}$  (JCPDS 37-629). It is likely that lattice strains were introduced by the existence of a Jahn-Teller one-sided Cu-centered octahedral structure in the HT layers [133]. These lattice strains could cause a decrease in peak intensity as observed for the 1.5-CuZnAl catalyst. Moreover, the crystallinity of the HT phases can be affected due to the generation of amorphous precipitates which are hydroxides in this case [93]. In addition, peaks with relatively weak intensity corresponding to metal oxide phases could also be detected for the catalysts. These species were most likely formed through the oxidation reaction due to the high aging temperature and pH. The peaks at  $2\theta$  of  $31.8^\circ$ ,  $36.3^\circ$ ,  $56.7^\circ$ ,  $63.0^\circ$ , and  $68.1^\circ$  can be attributed to ZnO (JCPDS 75-576), while the signal corresponding to CuO (JCPDS 89-5899) can be observed at  $32.5^\circ$ ,  $35.5^\circ$ ,  $38.8^\circ$  and  $48.7^\circ$ . The ZnO peaks had the highest intensity for

the 0.5-CuZnAl catalyst, which can be clearly seen from the peaks at 31.8° and 36.3°. However, the intensity of the ZnO peaks were very small for the 1-CuZnAl catalyst, indicating low degree of crystallization or high dispersion. Furthermore, the decrease in ZnO signal was accompanied by an increase in peak intensity of HT. It can also be observed that the intensity of the CuO peak at 38.8° increases with Cu loading, which was probably due to an increase in CuO crystallite size.

Structural properties of un-promoted catalysts are summarized in Table 4.1. The lattice parameter  $a$  ( $a = 2 \times d_{110}$ ) is a function of the average radius of the metal cations found in the layers while lattice parameter  $c$  ( $c = 3 \times d_{003}$ ) measures the HT's layer thickness [44, 93]. The d-spacing ( $d_{110}$  and  $d_{003}$ ) was calculated by Braggs equation (eq.2.1). The crystallite size of ZnO ( $d_{ZnO}$ ) and CuO ( $d_{CuO}$ ) was calculated by the Scherrer equation (eq.2.2). Cu content has clearly affected the structural parameters of different molar ratio catalysts. Parameter  $a$  was increasing due to the decrease in Cu content. The differences were small due to the similar ionic radii between  $Zn^{2+}$  and  $Cu^{2+}$  [134]. In addition, parameter  $c$  was increasing with increasing Cu content, due to the lower electrostatic interaction between the layers [100].

Table 4.1. Structural parameters of un-promoted as-prepared catalysts and calculated crystallite size

Catalyst	$a$ (Å)	$c$ (Å)	$d_{ZnO}$ (nm)	$d_{CuO}$ (nm)
1.5-CuZnAl	3.541	22.47	45	15
1-CuZnAl	3.545	22.62	–	13
0.5-CuZnAl	3.548	22.71	49	9

XRD patterns of the calcined un-promoted catalysts are shown in Figure 4.2 after thermal treatment at 500°C for 5 hours. It is clear that the HT structure was completely decomposed [135], ending up with a composition of mixed oxides of ZnO and CuO. No peaks of Al containing species were detected, which indicates that the Al exists as an amorphous phase. The crystallite size of ZnO and CuO was estimated by the Scherrer equation from the (100) and (111), respectively, and the values are listed in Table 4-1. As it can be seen, the crystallite size of ZnO was very large for the 0.5-CuZnAl and 1.5-CuZnAl catalysts, while the crystallite size could not be calculated for the 1-CuZnAl catalyst. It can also be seen that the CuO crystallite size increased with Cu loading in the range of 9-15 nm.

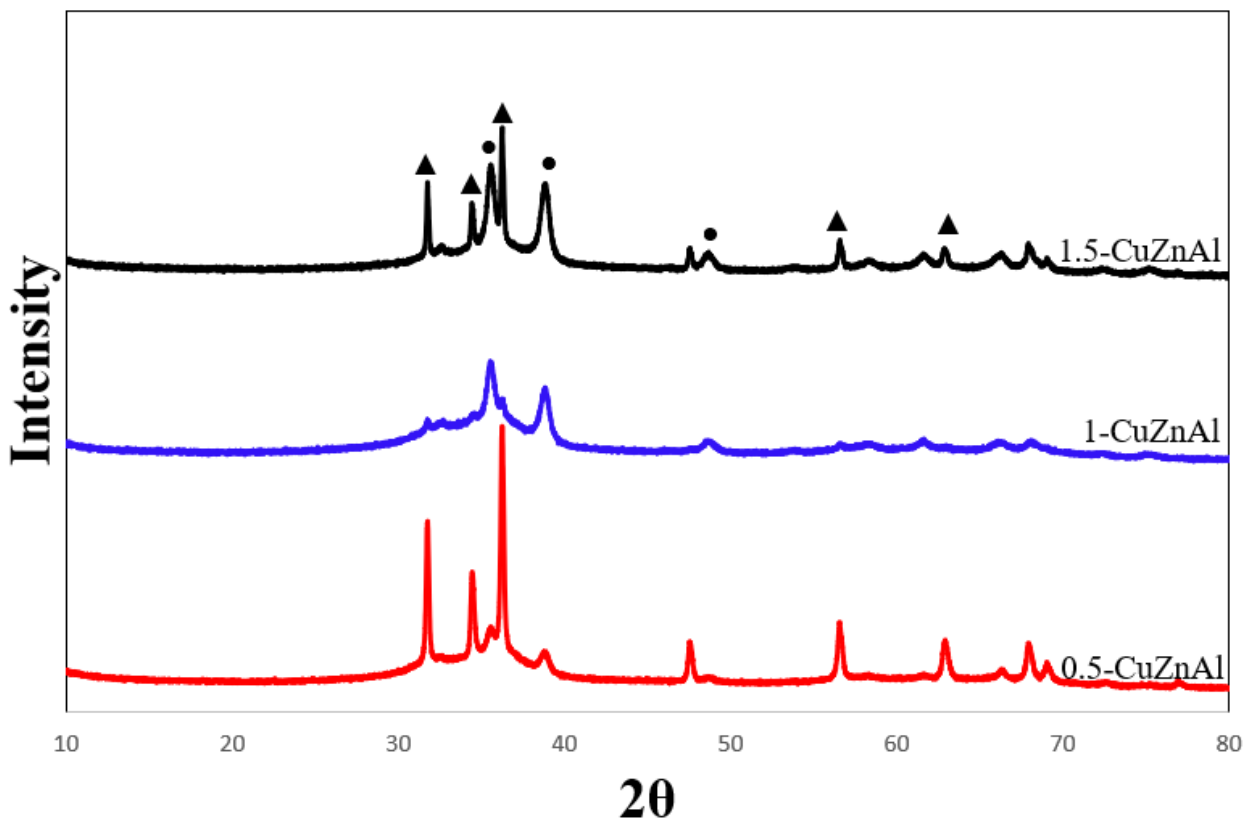


Figure 4.2. XRD patterns of un-promoted calcined catalysts, (▲) ZnO and (●) CuO

#### 4.1.2 XRD analysis of promoted catalysts

XRD patterns of the promoted catalyst precursors are presented in Figure 4.3. The patterns of In-promoted catalysts show the same HT pattern as the un-promoted catalyst, but with the addition of an  $\text{In}(\text{OH})_3$  structure (JCPDS 85-1338). The peaks at  $2\theta$  of  $22.7^\circ$  and  $32^\circ$  are characteristics of  $\text{In}(\text{OH})_3$ , and the peak intensity increased with In loading. The crystallinity of the promoted samples decreased with increasing  $\text{In}^{3+}$ , since  $\text{Al}^{3+}$  (ionic radius = 0.05 nm) was being substituted by  $\text{In}^{3+}$  (ionic radius = 0.081 nm) which has a larger ionic radius.

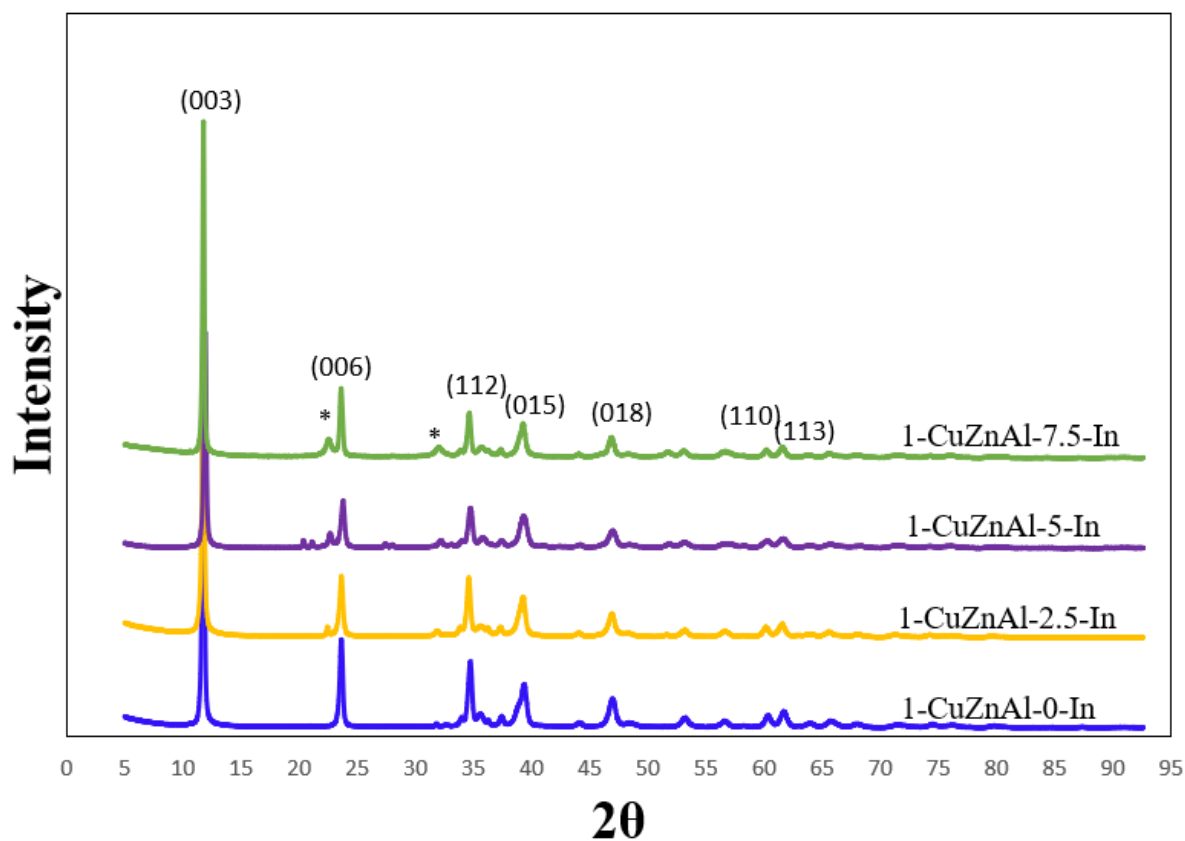


Figure 4.3. XRD patterns of promoted as-prepared catalysts, (\*) In (OH)<sub>3</sub>.

Structural properties of promoted catalysts are summarized in Table 4.2. Parameter  $a$  increased with the addition of In, which indicates that In was incorporated into the HT structure [91]. Parameter  $c$  of the promoted catalyst was found to be slightly larger than the un-promoted catalyst. This could be due to an increase in the  $M^{2+}/M^{3+}$  ratio of the HT layers causing the positive ionic charge density between the layers to decrease, thus increasing the  $M^{2+}-M^{3+}-O$  octahedron structure [136].

Table 4.2. Structural parameters of promoted as-prepared catalysts and calculated crystallite size

Catalyst	$a$ (Å)	$c$ (Å)	$d_{CuO}$ (nm)
1-CuZnAl-0-In	3.545	22.62	13
1-CuZnAl-2.5-In	3.549	22.65	11
1-CuZnAl-5-In	3.550	22.63	10
1-CuZnAl-7.5-In	3.551	22.63	10

XRD patterns of the calcined promoted catalysts are shown in Figure 4.4. It can be seen that the HT structure was completely decomposed after calcination, and that of the  $\text{In}(\text{OH})_3$  component has also disappeared. The crystalline size of Cu decreased with increasing In content, which indicates that In addition increased the Cu dispersion. In addition, according to Gao *et al.* [44] Cu nanoparticles are physically spaced by ZnO particles which helps in the dispersion of the Cu phase.

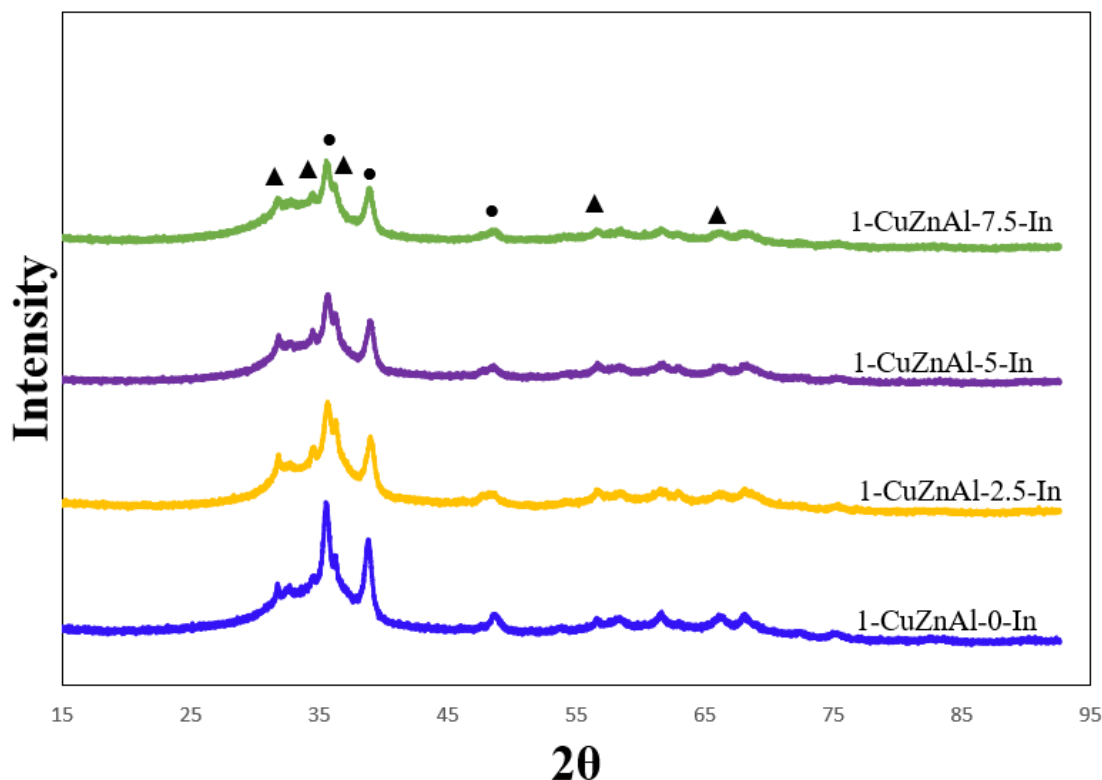


Figure 4.4. XRD patterns of promoted calcined catalysts, (▲) ZnO and (●) CuO

#### 4.1.3 TPR analysis

The reduction behavior of the calcined catalysts was studied using  $\text{H}_2$ -TPR and the results are presented in Figure 4.5. For the un-promoted catalysts, the high temperature peak represents the reduction of bulk CuO or Cu in mixed oxide phase, while the peak at low temperatures can be linked to the reduction of highly dispersed CuO [133]. Therefore, it appears that a larger fraction of CuO was present as highly dispersed species for the 1.5-CuZnAl catalyst. As expected, the peak intensity increased with the Cu loading due to the higher amount of reducible CuO. This was also confirmed by the calculation of  $\text{H}_2$ -consumption during TPR measurements, which is given in Table 4.3.

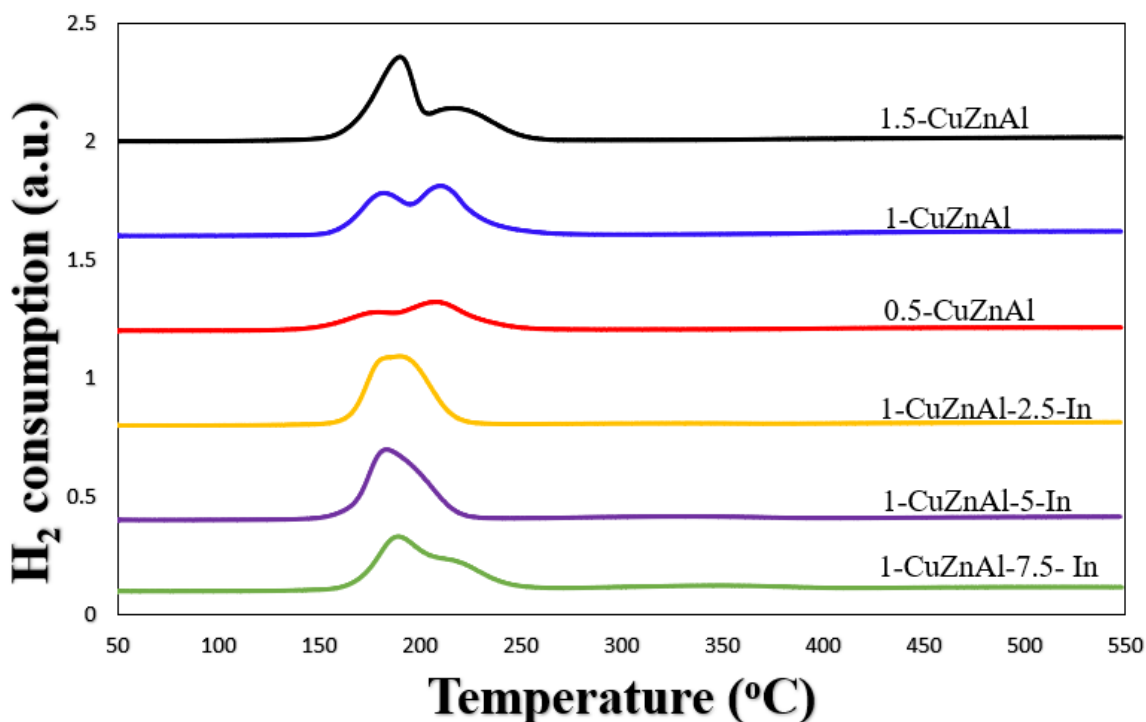


Figure 4.5. TPR profiles of calcined catalysts

It was observed that the reduction profile of In-promoted catalyst shifted towards lower temperatures compared to the un-promoted catalyst. This can be attributed to a higher amount of well-dispersed CuO [92]. The claim of the high amount of well-dispersed CuO can be supported by the XRD data of the promoted catalysts, which showed that the crystallite size of CuO was smaller and decreased with increasing In loading. However, the reducibility was better for the 1-CuZnAl-5-In catalyst and a higher temperature was required to reduce the 1-CuZnAl-7.5-In catalyst. From Table 4.3, it can be seen that the amount of reducible CuO species was not notably affected by the addition of In.

#### 4.1.4 N<sub>2</sub> adsorption-desorption

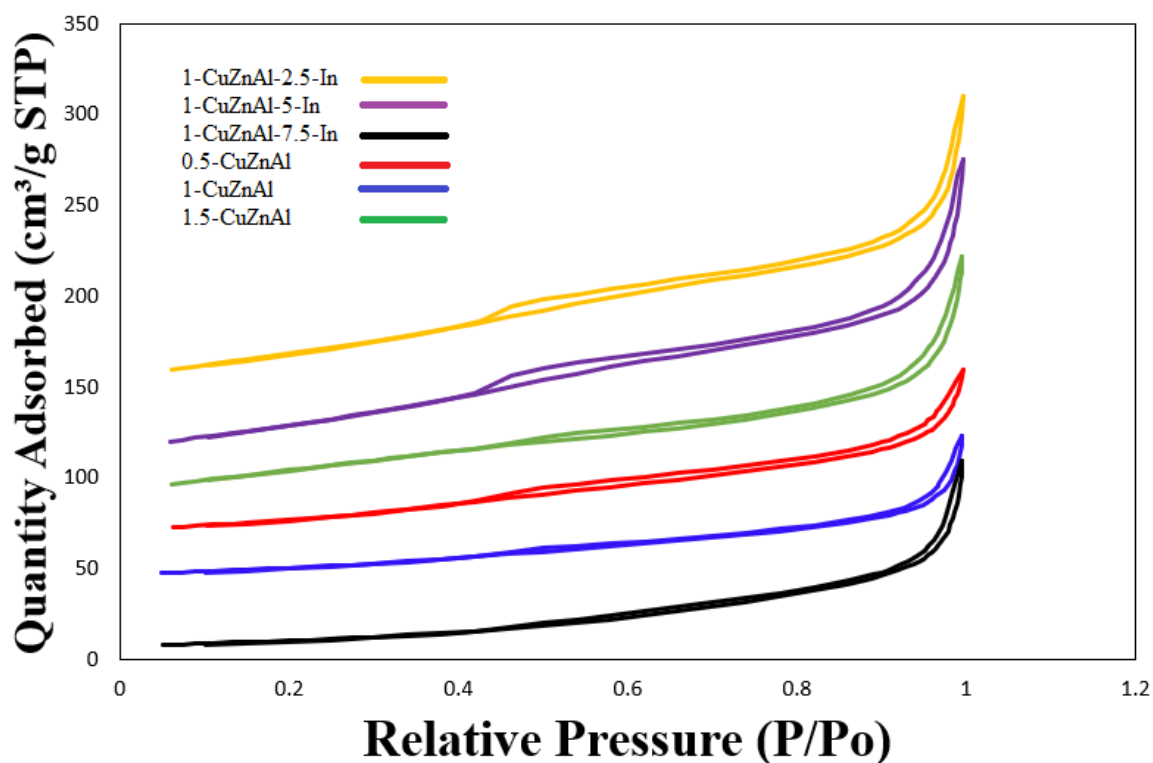


Figure 4.6. N<sub>2</sub> adsorption-desorption isotherms of calcined catalysts

The N<sub>2</sub> adsorption-desorption isotherms are shown in Figure 4.6. According to the IUPAC manual, the isotherm was of type IV with a hysteresis loop of type H3 [137], which indicates that the pores of catalysts were of mesoporous structure. The pore size distribution is presented in Figure 4.7, and the catalysts exhibit similar pore size distributions. Table 4.3 summarizes all the textural properties of the catalysts. The 0.5-CuZnAl showed the highest surface area (64 m<sup>2</sup>/g) among the un-promoted catalyst. Increasing the Cu/Zn ratio resulted in a decrease in surface area, where the 1-CuZnAl and 1.5-CuZnAl showed similar surface area of 38 m<sup>2</sup>/g and 39 m<sup>2</sup>/g, respectively. The pore volume was also comparable for the un-promoted catalysts in the range of 7-11 cm<sup>3</sup>/g. On the other hand, the In-promoted catalysts showed a significant increase in surface area and pore volume compared to the un-promoted catalysts. The In-promoted catalysts had comparable surface area of 112-117 m<sup>2</sup>/g. The pore volume of 1-CuZnAl-2.5-In and 1-CuZnAl-5-In was 0.17 cm<sup>3</sup>/g and 0.18 cm<sup>3</sup>/g respectively. A slight decrease in pore volume was observed for the 1-CuZnAl-7.5-In (0.13 cm<sup>3</sup>/g).



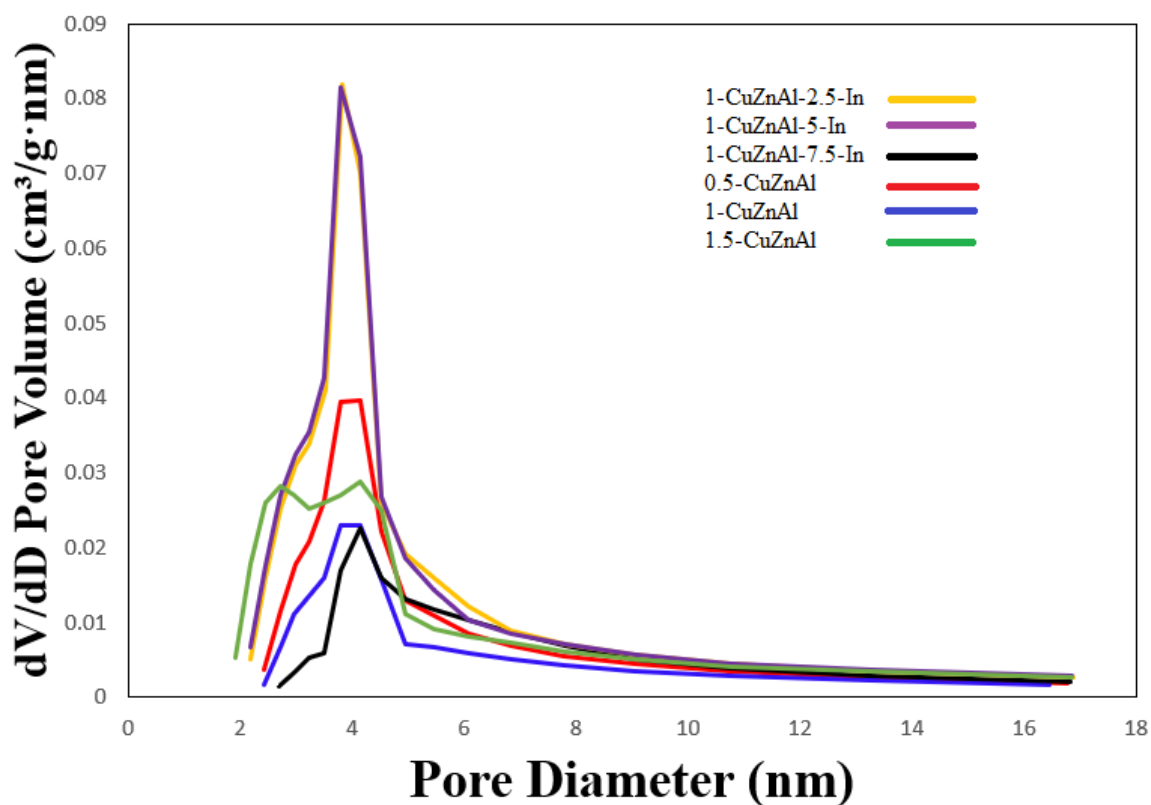


Figure 4.7. Pore size distribution of calcined catalysts

Table 4.3. Textual properties of calcined catalysts

Catalyst	BET Surface Area (m <sup>2</sup> /g)	BJH Pore Volume (cm <sup>3</sup> /g)	Pore size (nm)	H <sub>2</sub> consumption (mmol/g)
1.5-CuZnAl	38	0.9	4.2	5.5
1-CuZnAl	39	0.7	5.1	4.4
0.5-CuZnAl	64	0.11	4.0	2.7
1-CuZnAl-2.5-In	112	0.17	4.5	4.5
1-CuZnAl-5-In	116	0.18	4.5	4.6
1-CuZnAl-7.5-In	117	0.13	4.2	4.5

## 4.2 Methanol synthesis activity tests

### 4.2.1 Activity and selectivity of un-promoted catalysts

Methanol synthesis reactions for un-promoted catalysts were performed under a pressure of 30 bars, and a temperature of 250 °C for a 24 h time period, with a 50 mL/min gas flow having a H<sub>2</sub>/CO<sub>2</sub>/N<sub>2</sub> ratio of 3/1/1. The fluctuations in the CO<sub>2</sub> conversion and methanol selectivity can be attributed to a sum of measurements and reaction condition errors, which become more prominent at low CO<sub>2</sub> conversion. The CO<sub>2</sub> conversion and methanol selectivity over the un-promoted CuZnAl catalysts are presented in Figure 4.8 and the average results are summarized in Table 4.4. It can be observed that the CO<sub>2</sub> conversion increased with Cu loading, which can be attributed to a higher Cu surface area. The activity of the 0.5-CuZnAl and 1-CuZnAl was comparable at 12.9% and 11.5%, respectively. This might be due to the significantly higher surface area as well as the improvement in Cu dispersion of the 0.5-CuZnAl catalyst, which probably has resulted in a similar Cu surface area. A slight drop in CO<sub>2</sub> conversion was observed for the 0.5-CuZnAl and 1-CuZnAl catalyst in the first 3 hours, while the CO<sub>2</sub> conversion increase mildly for the 1.5-CuZnAl catalyst.

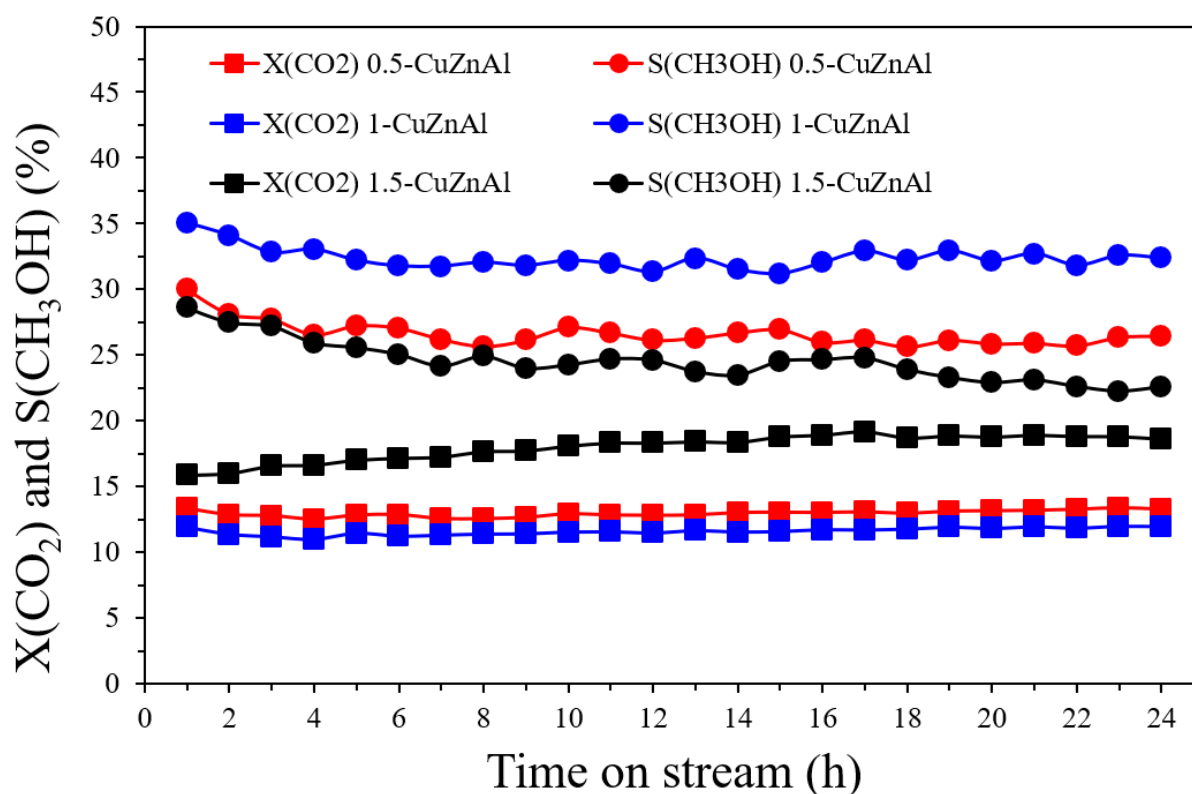


Figure 4.8. CO<sub>2</sub> conversion and CH<sub>3</sub>OH selectivity of CuZnAl catalysts

Table 4.4. Summary of average CO<sub>2</sub> conversion and CH<sub>3</sub>OH selectivity of un-promoted catalysts

Catalyst	CO <sub>2</sub> conversion (%)	CH <sub>3</sub> OH selectivity (%)
0.5-CuZnAl	12.9	26.7
1-CuZnAl	11.5	32.3
1.5-CuZnAl	17.8	24.8

The methanol selectivity is usually controlled by the competition between the two reactions of CO<sub>2</sub> hydrogenation to methanol (1) and the RWGS reaction (3) [138]. Hydrocarbons and other oxygenates could also be formed during CO<sub>2</sub> hydrogenation, but these species were not detected over the catalysts tested in this work (detection limit 0.1%). Therefore, since methanol and CO were the products that formed, only the methanol selectivity will be presented. It was found that the 1-CuZnAl catalyst achieved the highest methanol selectivity of 32.3%. The 0.5-CuZnAl and 1.5-CuZnAl exhibited comparable selectivity of 26.7% and 24.8%, respectively. The methanol selectivity dropped slightly during the first hours and then stabilized. Several studies have shown the importance of the Cu/ZnO interface to achieve high methanol selectivity [63, 139]. The 0.5-CuZnAl and 1.5-CuZnAl catalysts showed very large ZnO crystallite size, which might result in similar Cu/ZnO interaction. On the other hand, XRD indicated high dispersion or poor crystallization of ZnO for the 1-CuZnAl catalyst. This has probably resulted in a higher Cu/ZnO interfacial area, which increased the methanol selectivity.

#### 4.2.2 Activity and selectivity of promoted catalysts

After the initial testing of the CuZnAl catalysts, the 1-CuZnAl catalyst was chosen for In promotion. This was due to the higher dispersion of ZnO phase obtained for this catalyst, and the better catalytic performance. The promoted catalysts were tested under the exact conditions mentioned in section 4.2.1. The CO<sub>2</sub> conversion and methanol selectivity over 24 h is shown in Figure 4.9 and the averaged results are summarized in Table 4.5. The CO<sub>2</sub> conversion decreased with increasing In loading. In addition, it can be observed that the CO<sub>2</sub> conversion was rather stable for all catalysts. The methanol selectivity was found to improve with increasing In loading. The highest methanol selectivity was obtained over the 1-CuZnAl-5-In catalysts at 52.6%, while the 1-CuZnAl-2.5-In and 1-CuZnAl-7.5-In achieved a selectivity of 36.1% and 48.5%, respectively. This shows that a suitable amount of In can improve the

methanol selectivity of CuZnAl catalysts. The improvement in methanol selectivity can be ascribed to better Cu and ZnO dispersion, leading to enhanced Cu/ZnO interaction, and an improvement in CuO reducibility. The methanol selectivity remained relatively stable for all catalysts after an initial slight decrease.

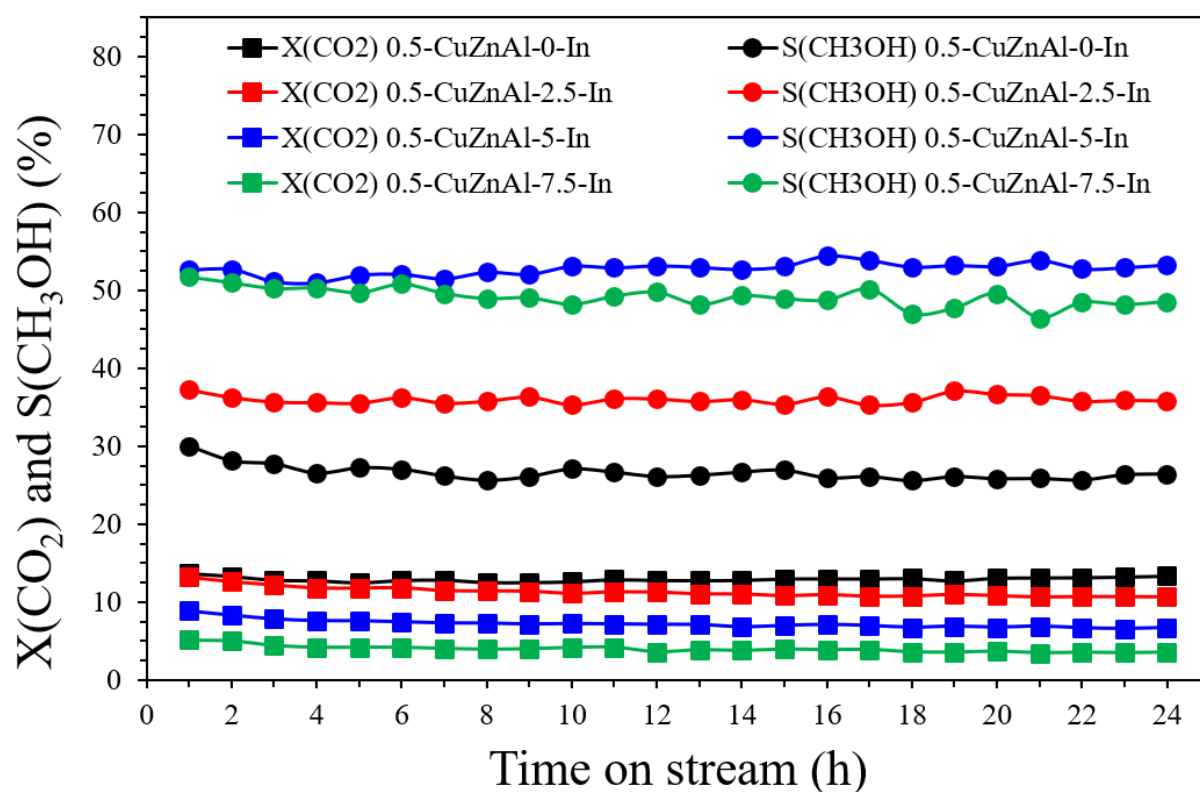


Figure 4.9. CO<sub>2</sub> conversion and CH<sub>3</sub>OH selectivity of promoted CuZnAl catalysts

Table 4.5. Summary of average CO<sub>2</sub> conversion and CH<sub>3</sub>OH selectivity of promoted catalysts

Catalyst	CO <sub>2</sub> conversion (%)	CH <sub>3</sub> OH selectivity (%)
1-CuZnAl- In	11.5	32.3
1-CuZnAl-2.5 In	11.4	36.1
1-CuZnAl-5 In	7.3	52.6
1-CuZnAl-7.5 In	3.9	48.5

#### 4.2.3 Temperature effect on the 1-CuZnAl-5-In and 1-CuZnAl-0-In catalysts

The effect of temperature was investigated over the 1-CuZnAl-5-In and 1-CuZnAl-0-In catalysts by changing the temperature from 230°C to 260°C stepwise at 10 °C per step. Each

temperature was maintained for approximately 6 h. The CO<sub>2</sub> conversion and methanol selectivity at different temperatures are presented in Figure 4.10. The CO<sub>2</sub> conversion increased more strongly with temperature for the 1-CuZnAl-0-In catalyst. The CO<sub>2</sub> conversion obtained over the 1-CuZnAl-0-In catalyst was 5.8% at 230 °C and increased to 14.7% at 260 °C. For 1-CuZnAl-5-In, the CO<sub>2</sub> conversion increased from 5.1% at 230 °C and to 9.5% at 260°C. The difference in CO<sub>2</sub> conversion between the catalysts could be related to the active sites, where the active sites for the RWGS reaction has been suppressed by the addition of In.

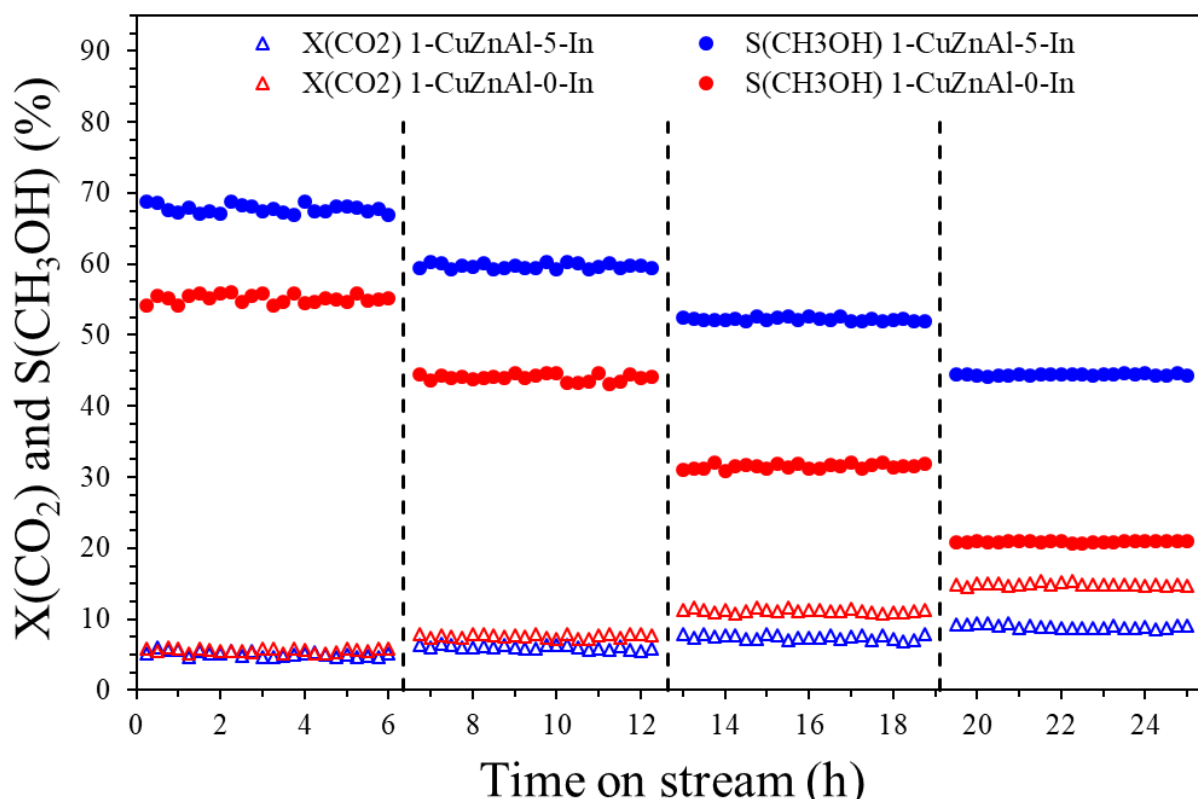


Figure 4.10. Effect of temperature on CO<sub>2</sub> conversion and CH<sub>3</sub>OH selectivity on 1-CuZnAl-5-In and 1-CuZnAl-0-In catalysts

The methanol selectivity decreased with temperature over both catalysts due to the RWGS reaction, which becomes more favorable at higher temperatures. The methanol selectivity decreased from 54.3% at 230 °C to 21.1% at 260 °C over the 1-CuZnAl-0-In catalyst. In contrast, the methanol selectivity remained higher throughout the temperature range for 1-CuZnAl-5-In, where the selectivity dropped from 67.9% at 230°C and to 44.3% at 260°C. The decrease in methanol selectivity for the In-promoted catalyst was significantly smaller than for the un-promoted catalyst. This could be due to the improvement in dispersion of species and a higher Cu/ZnO interfacial area. In addition, the In species might also have contributed as it has

been showed that In based catalysts can maintain a higher methanol selectivity even at temperatures up to 300 °C [18, 19].

#### 4.2.4 Long run reactions

Long term stability is essential for a catalyst to be viable in industrial applications. Based on the experimental results, the 1-CuZnAl-5-In catalyst was chosen for the stability test and 1-CuZnAl-0-In was also tested for comparison. These tests were carried out at the same reaction conditions as described in sections 4.2.1 but the reaction period was increased from 24 h to 72 h. The CO<sub>2</sub> conversion and methanol selectivity over 72 h time on stream are presented in Figure 4.11. For 1-CuZnAl-0-In catalyst, the CO<sub>2</sub> conversion increased steadily over the reaction period. Initially, the CO<sub>2</sub> conversion was 11.9% and it increased to 14.1% after 72 h. On the other hand, the methanol selectivity decreased by 10.6% where it started at 35.1% and reached 24.5% at the end of the reaction period. These results suggest that the deactivation could be related to a reduction in Cu/ZnO<sub>x</sub> interfacial area, which has been shown to be linked to the methanol selectivity [44]. The reduction of Cu/ZnO<sub>x</sub> interfacial area might be due to particle sintering. The CO<sub>2</sub> conversion of 1-CuZnAl-5-In was initially 8.6% and it decreased in the beginning before it stabilized at approximately 5.9% after around 32 h. In contrast, the methanol selectivity improved slightly before it stabilized at approximately 53.5%. It can be seen that In promotion of HT-derived CuZnAl catalysts can significantly improve the stability of the catalyst in CO<sub>2</sub> hydrogenation to methanol. The exact reason for the higher stability of the In containing catalyst is not known at the present. It could be related to the improvement in dispersion and In having a stabilizing effect on the catalytic structure.

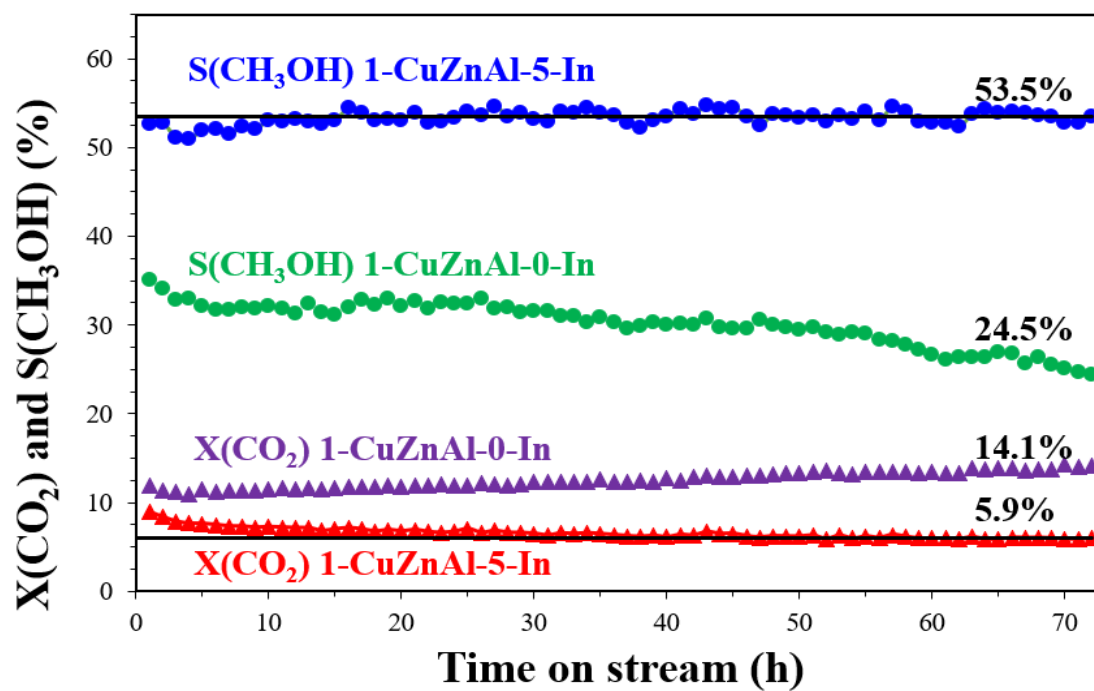


Figure 4.11.  $\text{CO}_2$  conversion and methanol selectivity over the 1-CuZnAl-5-In catalyst for 72 h TOS. The black lines indicate the average  $\text{CO}_2$  conversion and methanol selectivity of the last 1 hour.

## 5 Conclusions and future work

### 5.1 Conclusions

In this study, catalytic hydrogenation of CO<sub>2</sub> to methanol was investigated using Cu/ZnO/Al<sub>2</sub>O<sub>3</sub> catalysts synthesized from hydrotalcite (HT) precursors. The focus of this study was to examine the effect of different molar ratios Cu/Zn (0.5, 1.0, 1.5) on the catalytic performance and investigate the effect of In promotion. The In-promoted catalysts had a fixed Cu/Zn ratio of 1 and an In content of 2.5, 5.0, 7.5 mol%.

Structural and textural characterization were conducted by XRD, TPR, and N<sub>2</sub> adsorption-desorption and demonstrated the following:

- The un-promoted and promoted catalysts exhibited a typical hydrotalcite structure with the presence of In(OH)<sub>3</sub> phase in the promoted catalysts.
- The lattice parameters of the un-promoted hydrotalcite precursors increased with decreasing Cu content.
- An increase in lattice parameters for the promoted catalysts indicated that parts of the In was incorporated into the HT structure.
- Crystallite size of CuO in the un-promoted calcined catalyst increased with Cu loading
- The introduction of In to 1-Cu/ZnO/Al<sub>2</sub>O<sub>3</sub> decreased the crystallite size of CuO.
- In promotion significantly increased surface area and pore volume of the catalyst.
- In promotion improved the reducibility and shifted the reduction of CuO towards lower temperatures

Activity and methanol selectivity of the catalysts were examined at 250°C and 30 bars for a 24 h period. It was observed that the CO<sub>2</sub> conversion increased for high Cu content. The 1-Cu/ZnO/Al<sub>2</sub>O<sub>3</sub> catalyst achieved the highest methanol selectivity of 32.3% at 11.5% CO<sub>2</sub> conversion of the un-promoted catalysts. Therefore, a Cu/Zn ratio of 1 was chosen for synthesizing the In-promoted catalysts. The CO<sub>2</sub> conversion decreased with increasing In loading, while the methanol selectivity was significantly improved. The highest methanol selectivity was obtained over the 1-CuZnAl-5-In catalyst at 52.6% with a CO<sub>2</sub> conversion of 7.3%. The effect of temperature was investigated over the 1-CuZnAl-5-In and the 1-CuZnAl-0-In catalysts by changing the temperature from 230°C to 260 °C stepwise at 10 °C per step. The 1-CuZnAl-5-In catalyst achieved a higher methanol selectivity that remained high even at 260 °C. In contrast, the methanol selectivity of 1-CuZnAl-0-In decreased significantly with



increasing temperature. Furthermore, long term tests of 1-CuZnAl-0-In and 1-CuZnAl-5-In demonstrated that the catalytic stability was also significantly improved by In promotion.

## **5.2 Recommendations for future work**

Additional work must be done to consider the use of In as a promoter to the Cu/ZnO/Al<sub>2</sub>O<sub>3</sub> catalyst. Although the use of 5 mol% In resulted in relatively high catalytic performance in terms of methanol selectivity and stability, different amounts of In between 2.5 mol% and 5 mol% should be examined to determine the optimum In loading.

The effect of In on the reaction mechanism should also be investigated. This could be done by a detailed kinetic study combined with in-situ characterization of surface species during methanol synthesis. In addition, DFT calculations can be used to gain information on the intermolecular interactions between components and the reaction's mechanism. This information could then be used to design improved catalysts by adjusting the interaction between species through the tuning of preparation methods. The focus should be to further improve the methanol selectivity while at the same time maintaining or enhancing the activity of the catalyst. Furthermore, the stability of the improved catalyst should be investigated over a longer reaction period to determine the applicability for industrial methanol synthesis from CO<sub>2</sub>.

## 6 References

- [1] IPCC, "Climate Change 2013: The Physical Science Basis,," *Intergovernmental Panel on Climate Change*, 2013. [Online]. Available: <https://www.ipcc.ch/report/ar5/wg1/>.
- [2] C. Le Quéré *et al.*, "Global Carbon Budget 2018," *Earth Syst. Sci. Data*, vol. 10, no. 4, pp. 2141-2194, 2018, doi: 10.5194/essd-10-2141-2018.
- [3] A. Raza, R. Gholami, R. Rezaee, V. Rasouli, and M. Rabiei, "Significant aspects of carbon capture and storage – A review," *Petroleum*, 2018/12/19/ 2018, doi: <https://doi.org/10.1016/j.petlm.2018.12.007>.
- [4] D. J. Peter Styring "Carbon Capture and Utilisation in the green economy," The University of Sheffield, 501, 2011. [Online]. Available: <https://static1.squarespace.com/static/5705589f7c65e48e7d7aae7f/t/57ae082d3e00be9be5dd11b1/1471023153349/CCU+carbon+capture+ideas.pdf>
- [5] G. A. Olah, "Beyond Oil and Gas: The Methanol Economy," *Angewandte Chemie International Edition*, vol. 44, no. 18, pp. 2636-2639, 2005/04/29 2005, doi: 10.1002/anie.200462121.
- [6] G. Bozzano and F. Manenti, "Efficient methanol synthesis: Perspectives, technologies and optimization strategies," *Progress in Energy and Combustion Science*, vol. 56, pp. 71-105, 2016, doi: 10.1016/j.pecs.2016.06.001.
- [7] I. Ganesh, "Conversion of carbon dioxide into methanol – a potential liquid fuel: Fundamental challenges and opportunities (a review)," *Renewable and Sustainable Energy Reviews*, vol. 31, pp. 221-257, 2014, doi: 10.1016/j.rser.2013.11.045.
- [8] G. A. Olah, A. Goepfert, and G. S. Prakash, "Chemical recycling of carbon dioxide to methanol and dimethyl ether: from greenhouse gas to renewable, environmentally carbon neutral fuels and synthetic hydrocarbons," *The Journal of organic chemistry*, vol. 74, no. 2, pp. 487-498, 2008.
- [9] K. Zhao, "A Brief Review of China's Methanol Vehicle Pilot and Policy ", 20 March 2019 2019. [Online]. Available: <https://www.methanol.org/wp-content/uploads/2019/03/A-Brief-Review-of-Chinas-Methanol-Vehicle-Pilot-and-Policy-20-March-2019.pdf>
- [10] M. Alvarado. "The changing face of the global methanol industry." IHS Markit. <https://chemweek.com/CW/Document/80172/The-changing-face-of-the-global-methanol-industry> (accessed).
- [11] I. U. Din, M. S. Shaharun, M. A. Alotaibi, A. I. Alharthi, and A. Naeem, "Recent developments on heterogeneous catalytic CO<sub>2</sub> reduction to methanol," *Journal of CO<sub>2</sub>*

*Utilization*, vol. 34, pp. 20-33, 2019/12/01/ 2019, doi: <https://doi.org/10.1016/j.jcou.2019.05.036>.

[12] G. Centi and S. Perathoner, *Green carbon dioxide : advances in CO2 utilization*, Hoboken, New Jersey: Wiley, 2014.

[13] D. Brat, "Catalytic CO2 Hydrogenation - Literature Review:

Technology Development since 2014," 2016. [Online]. Available: <https://pdfs.semanticscholar.org/c7bf/b16cfade23e09546784a92c89928671e6ce8.pdf>.

[14] S. Dang *et al.*, "A review of research progress on heterogeneous catalysts for methanol synthesis from carbon dioxide hydrogenation," *Catalysis Today*, 2018, doi: 10.1016/j.cattod.2018.04.021.

[15] J. Toyir, P. R. r. de la Piscina, J. L. G. Fierro, and N. s. Homs, "Highly effective conversion of CO2 to methanol over supported and promoted copper-based catalysts: influence of support and promoter," *Applied Catalysis B: Environmental*, vol. 29, no. 3, pp. 207-215, 2001/02/01/ 2001, doi: [https://doi.org/10.1016/S0926-3373\(00\)00205-8](https://doi.org/10.1016/S0926-3373(00)00205-8).

[16] K. Klier, V. Chatikavanij, R. G. Herman, and G. W. Simmons, "Catalytic synthesis of methanol from COH2: IV. The effects of carbon dioxide," *Journal of Catalysis*, vol. 74, no. 2, pp. 343-360, 1982/04/01/ 1982, doi: [https://doi.org/10.1016/0021-9517\(82\)90040-9](https://doi.org/10.1016/0021-9517(82)90040-9).

[17] U. Costantino *et al.*, "Cu–Zn–Al hydrotalcites as precursors of catalysts for the production of hydrogen from methanol," *Solid State Ionics*, vol. 176, no. 39, pp. 2917-2922, 2005/12/01/ 2005, doi: <https://doi.org/10.1016/j.ssi.2005.09.051>.

[18] M. S. Frei *et al.*, "Mechanism and microkinetics of methanol synthesis via CO2 hydrogenation on indium oxide," *Journal of Catalysis*, vol. 361, pp. 313-321, 2018, doi: 10.1016/j.jcat.2018.03.014.

[19] O. Martin *et al.*, "Indium Oxide as a Superior Catalyst for Methanol Synthesis by CO2 Hydrogenation," *Angewandte Chemie International Edition*, vol. 55, no. 21, pp. 6261-6265, 2016, doi: 10.1002/anie.201600943.

[20] N. Rui, Z. Wang, K. Sun, J. Ye, Q. Ge, and C.-j. Liu, "CO2 hydrogenation to methanol over Pd/In2O3: effects of Pd and oxygen vacancy," *Applied Catalysis B: Environmental*, vol. 218, pp. 488-497, 2017/12/05/ 2017, doi: <https://doi.org/10.1016/j.apcatb.2017.06.069>.

[21] J. Ye, C.-j. Liu, D. Mei, and Q. Ge, "Methanol synthesis from CO2 hydrogenation over a Pd4/In2O3 model catalyst: A combined DFT and kinetic study," *Journal of Catalysis*, vol. 317, pp. 44-53, 2014/08/01/ 2014, doi: <https://doi.org/10.1016/j.jcat.2014.06.002>.

- [22] S. G. Jadhav, P. D. Vaidya, B. M. Bhanage, and J. B. Joshi, "Catalytic carbon dioxide hydrogenation to methanol: A review of recent studies," (in English), *Chem Eng Res Des*, vol. 92, no. 11, pp. 2557-2567, Nov 2014, doi: 10.1016/j.cherd.2014.03.005.
- [23] S. K. Wilkinson, L. G. A. van de Water, B. Miller, M. J. H. Simmons, E. H. Stitt, and M. J. Watson, "Understanding the generation of methanol synthesis and water gas shift activity over copper-based catalysts – A spatially resolved experimental kinetic study using steady and non-steady state operation under CO/CO<sub>2</sub>/H<sub>2</sub> feeds," *Journal of Catalysis*, vol. 337, pp. 208-220, 2016, doi: 10.1016/j.jcat.2016.01.025.
- [24] J. M. Thomas, *Principles and practice of heterogeneous catalysis*, W. J. Thomas, ed., 2nd ed. ed. Weinheim, Germany: Wiley-VCH, 2015.
- [25] K. Stangeland, H. Li, and Z. Yu, "Thermodynamic Analysis of Chemical and Phase Equilibria in CO<sub>2</sub> Hydrogenation to Methanol, Dimethyl Ether, and Higher Alcohols," *Industrial & Engineering Chemistry Research*, vol. 57, no. 11, pp. 4081-4094, 2018, doi: 10.1021/acs.iecr.7b04866.
- [26] K. Stangeland, H. Li, and Z. Yu, "Thermodynamic Analysis of Chemical and Phase Equilibria in CO<sub>2</sub> Hydrogenation to Methanol, Dimethyl Ether, and Higher Alcohols," *Industrial & Engineering Chemistry Research*, vol. 57, no. 11, pp. 4081-4094, 2018, doi: 10.1021/acs.iecr.7b04866.
- [27] Y. Yang, C. A. Mims, R. S. Disselkamp, J.-H. Kwak, C. H. F. Peden, and C. T. Campbell, "(Non)formation of Methanol by Direct Hydrogenation of Formate on Copper Catalysts," *The Journal of Physical Chemistry C*, vol. 114, no. 40, pp. 17205-17211, 2010/10/14 2010, doi: 10.1021/jp104068k.
- [28] M. B. Fichtl *et al.*, "Kinetics of deactivation on Cu/ZnO/Al<sub>2</sub>O<sub>3</sub> methanol synthesis catalysts," *Applied Catalysis A, General*, vol. 502, pp. 262-270, 2015, doi: 10.1016/j.apcata.2015.06.014.
- [29] Y.-F. Zhao, Y. Yang, C. Mims, C. H. F. Peden, J. Li, and D. Mei, "Insight into methanol synthesis from CO<sub>2</sub> hydrogenation on Cu(1 1 1): Complex reaction network and the effects of H<sub>2</sub>O," *Journal of Catalysis*, vol. 281, no. 2, pp. 199-211, 2011, doi: 10.1016/j.jcat.2011.04.012.
- [30] F. Arena, K. Barbera, G. Italiano, G. Bonura, L. Spadaro, and F. Frusteri, "Synthesis, characterization and activity pattern of Cu–ZnO/ZrO<sub>2</sub> catalysts in the hydrogenation of carbon dioxide to methanol," *Journal of Catalysis*, vol. 249, no. 2, pp. 185-194, 2007/07/25/ 2007, doi: <https://doi.org/10.1016/j.jcat.2007.04.003>.

- [31] S.-i. Fujita, S. Moribe, Y. Kanamori, M. Kakudate, and N. Takezawa, "Preparation of a coprecipitated Cu/ZnO catalyst for the methanol synthesis from CO<sub>2</sub> — effects of the calcination and reduction conditions on the catalytic performance," *Applied Catalysis A: General*, vol. 207, no. 1, pp. 121-128, 2001/02/01/ 2001, doi: [https://doi.org/10.1016/S0926-860X\(00\)00616-5](https://doi.org/10.1016/S0926-860X(00)00616-5).
- [32] W. Ding *et al.*, "Promoting effect of a Cu–Zn binary precursor on a ternary Cu–Zn–Al catalyst for methanol synthesis from synthesis gas," *RSC Advances*, 10.1039/C4RA01583E vol. 4, no. 58, pp. 30677-30682, 2014, doi: 10.1039/C4RA01583E.
- [33] N. J. Brown, J. Weiner, K. Hellgardt, M. S. P. Shaffer, and C. K. Williams, "Phosphinate stabilised ZnO and Cu colloidal nanocatalysts for CO<sub>2</sub> hydrogenation to methanol," *Chemical Communications*, 10.1039/C3CC46203J vol. 49, no. 94, pp. 11074-11076, 2013, doi: 10.1039/C3CC46203J.
- [34] M. D. Rhodes and A. T. Bell, "The effects of zirconia morphology on methanol synthesis from CO and H<sub>2</sub> over Cu/ZrO<sub>2</sub> catalysts: Part I. Steady-state studies," *Journal of Catalysis*, vol. 233, no. 1, pp. 198-209, 2005/07/01/ 2005, doi: <https://doi.org/10.1016/j.jcat.2005.04.026>.
- [35] I. A. Fisher and A. T. Bell, "In Situ Infrared Study of Methanol Synthesis from H<sub>2</sub>/CO over Cu/SiO<sub>2</sub> and Cu/ZrO<sub>2</sub>/SiO<sub>2</sub>," *Journal of Catalysis*, vol. 178, no. 1, pp. 153-173, 1998/08/15/ 1998, doi: <https://doi.org/10.1006/jcat.1998.2134>.
- [36] J. Toyir *et al.*, "Sustainable process for the production of methanol from CO<sub>2</sub> and H<sub>2</sub> using Cu/ZnO-based multicomponent catalyst," *Physics Procedia*, vol. 2, no. 3, pp. 1075-1079, 2009/11/01/ 2009, doi: <https://doi.org/10.1016/j.phpro.2009.11.065>.
- [37] M. M.-J. Li, Z. Zeng, F. Liao, X. Hong, and S. C. E. Tsang, "Enhanced CO<sub>2</sub> hydrogenation to methanol over CuZn nanoalloy in Ga modified Cu/ZnO catalysts," *Journal of Catalysis*, vol. 343, pp. 157-167, 2016/11/01/ 2016, doi: <https://doi.org/10.1016/j.jcat.2016.03.020>.
- [38] O. Martin, C. Mondelli, D. Curulla-Ferré, C. Drouilly, R. Hauert, and J. Pérez-Ramírez, "Zinc-Rich Copper Catalysts Promoted by Gold for Methanol Synthesis," *ACS Catalysis*, vol. 5, no. 9, pp. 5607-5616, 2015/09/04 2015, doi: 10.1021/acscatal.5b00877.
- [39] S. Köhl, A. Tarasov, S. Zander, I. Kasatkin, and M. Behrens, "Cu-Based Catalyst Resulting from a Cu,Zn,Al Hydrotalcite-Like Compound: A Microstructural, Thermoanalytical, and In Situ XAS Study," *Chemistry – A European Journal*, vol. 20, no. 13, pp. 3782-3792, 2014, doi: 10.1002/chem.201302599.

- [40] S. Kühn, A. Tarasov, S. Zander, I. Kasatkin, and M. Behrens, "Cu - Based Catalyst Resulting from a Cu,Zn,Al Hydrotalcite - Like Compound: A Microstructural, Thermoanalytical, and In Situ XAS Study," *Chemistry – A European Journal*, vol. 20, no. 13, pp. 3782-3792, 2014, doi: 10.1002/chem.201302599.
- [41] P. Gao *et al.*, "Fluorinated Cu/Zn/Al/Zr hydrotalcites derived nanocatalysts for CO<sub>2</sub> hydrogenation to methanol," *Journal of CO<sub>2</sub> Utilization*, vol. 16, pp. 32-41, 2016/12/01/ 2016, doi: <https://doi.org/10.1016/j.jcou.2016.06.001>.
- [42] P. Gao *et al.*, "Influence of fluorine on the performance of fluorine-modified Cu/Zn/Al catalysts for CO<sub>2</sub> hydrogenation to methanol," *Journal of CO<sub>2</sub> Utilization*, vol. 2, pp. 16-23, 2013/09/01/ 2013, doi: <https://doi.org/10.1016/j.jcou.2013.06.003>.
- [43] P. Gao *et al.*, "Fluorine-modified Cu/Zn/Al/Zr catalysts via hydrotalcite-like precursors for CO<sub>2</sub> hydrogenation to methanol," *Catalysis Communications*, vol. 50, pp. 78-82, 2014/05/05/ 2014, doi: <https://doi.org/10.1016/j.catcom.2014.03.006>.
- [44] P. Gao *et al.*, "Yttrium oxide modified Cu/ZnO/Al<sub>2</sub>O<sub>3</sub> catalysts via hydrotalcite-like precursors for CO<sub>2</sub> hydrogenation to methanol," *Catalysis Science & Technology*, 10.1039/C5CY00372E vol. 5, no. 9, pp. 4365-4377, 2015, doi: 10.1039/C5CY00372E.
- [45] P. Gao, F. Li, N. Zhao, H. Wang, W. Wei, and Y.-H. Sun, "Preparation of Cu/Zn/Al/(Zr)/(Y) Catalysts from Hydrotalcite-Like Precursors and Their Catalytic Performance for the Hydrogenation of CO<sub>2</sub> to Methanol," *Acta Physico-Chimica Sinica*, vol. 30, no. 6, pp. 1155-1162, // 2014, doi: 10.3866/PKU.WHXB201401252.
- [46] K. Samson *et al.*, "Influence of ZrO<sub>2</sub> Structure and Copper Electronic State on Activity of Cu/ZrO<sub>2</sub> Catalysts in Methanol Synthesis from CO<sub>2</sub>," *ACS Catal.*, vol. 4, no. 10, pp. 3730-3741, 2014, doi: 10.1021/cs500979c.
- [47] I. Ro *et al.*, "Role of the Cu-ZrO<sub>2</sub> Interfacial Sites for Conversion of Ethanol to Ethyl Acetate and Synthesis of Methanol from CO<sub>2</sub> and H<sub>2</sub>," *ACS Catalysis*, vol. 6, no. 10, pp. 7040-7050, 2016/10/07 2016, doi: 10.1021/acscatal.6b01805.
- [48] B. Rungtaweivoranit *et al.*, "Copper Nanocrystals Encapsulated in Zr-based Metal–Organic Frameworks for Highly Selective CO<sub>2</sub> Hydrogenation to Methanol," *Nano Letters*, vol. 16, no. 12, pp. 7645-7649, 2016/12/14 2016, doi: 10.1021/acs.nanolett.6b03637.
- [49] B. An, J. Zhang, K. Cheng, P. Ji, C. Wang, and W. Lin, "Confinement of Ultrasmall Cu/ZnO<sub>x</sub> Nanoparticles in Metal–Organic Frameworks for Selective Methanol Synthesis from Catalytic Hydrogenation of CO<sub>2</sub>," *Journal of the American Chemical Society*, vol. 139, no. 10, pp. 3834-3840, 2017/03/15 2017, doi: 10.1021/jacs.7b00058.

- [50] E. L. Fornero, A. L. Bonivardi, and M. A. Baltanás, "Isotopic study of the rates of hydrogen provision vs. methanol synthesis from CO<sub>2</sub> over Cu–Ga–Zr catalysts," *Journal of Catalysis*, vol. 330, pp. 302-310, 2015/10/01/ 2015, doi: <https://doi.org/10.1016/j.jcat.2015.07.025>.
- [51] L. Mayr, X. Shi, N. Köpfle, B. Klötzer, D. Y. Zemlyanov, and S. Penner, "Tuning of the copper–zirconia phase boundary for selectivity control of methanol conversion," *Journal of Catalysis*, vol. 339, pp. 111-122, 2016/07/01/ 2016, doi: <https://doi.org/10.1016/j.jcat.2016.03.029>.
- [52] S. D. Senanayake *et al.*, "Hydrogenation of CO<sub>2</sub> to Methanol on CeO<sub>x</sub>/Cu(111) and ZnO/Cu(111) Catalysts: Role of the Metal–Oxide Interface and Importance of Ce<sup>3+</sup> Sites," *The Journal of Physical Chemistry C*, vol. 120, no. 3, pp. 1778-1784, 2016/01/28 2016, doi: 10.1021/acs.jpcc.5b12012.
- [53] N. Kumari, M. A. Haider, M. Agarwal, N. Sinha, and S. Basu, "Role of Reduced CeO<sub>2</sub>(110) Surface for CO<sub>2</sub> Reduction to CO and Methanol," *The Journal of Physical Chemistry C*, vol. 120, no. 30, pp. 16626-16635, 2016/08/04 2016, doi: 10.1021/acs.jpcc.6b02860.
- [54] Y. Bao *et al.*, "Highly efficient Cu/anatase TiO<sub>2</sub> {001}-nanosheets catalysts for methanol synthesis from CO<sub>2</sub>," *Journal of Energy Chemistry*, vol. 27, no. 2, pp. 381-388, 2018/03/01/ 2018, doi: <https://doi.org/10.1016/j.jechem.2017.12.015>.
- [55] K. Chen *et al.*, "CO<sub>2</sub> hydrogenation to methanol over Cu catalysts supported on La-modified SBA-15: The crucial role of Cu–LaO<sub>x</sub> interfaces," *Applied Catalysis B: Environmental*, vol. 251, pp. 119-129, 2019/08/15/ 2019, doi: <https://doi.org/10.1016/j.apcatb.2019.03.059>.
- [56] A. B. Vidal *et al.*, "CO<sub>2</sub> Activation and Methanol Synthesis on Novel Au/TiC and Cu/TiC Catalysts," *The Journal of Physical Chemistry Letters*, vol. 3, no. 16, pp. 2275-2280, 2012/08/16 2012, doi: 10.1021/jz300989e.
- [57] C. Kunkel, F. Viñes, and F. Illas, "Transition metal carbides as novel materials for CO<sub>2</sub> capture, storage, and activation," *Energy & Environmental Science*, 10.1039/C5EE03649F vol. 9, no. 1, pp. 141-144, 2016, doi: 10.1039/C5EE03649F.
- [58] S. Posada-Pérez *et al.*, "Highly Active Au/ $\delta$ -MoC and Cu/ $\delta$ -MoC Catalysts for the Conversion of CO<sub>2</sub>: The Metal/C Ratio as a Key Factor Defining Activity, Selectivity, and Stability," *Journal of the American Chemical Society*, vol. 138, no. 26, pp. 8269-8278, 2016/07/06 2016, doi: 10.1021/jacs.6b04529.

- [59] J. B. Branco, A. C. Ferreira, A. P. Gonçalves, C. O. Soares, and T. Almeida Gasche, "Synthesis of methanol using copper–f block element bimetallic oxides as catalysts and greenhouse gases (CO<sub>2</sub>, CH<sub>4</sub>) as feedstock," *Journal of Catalysis*, vol. 341, pp. 24-32, 2016/09/01/ 2016, doi: <https://doi.org/10.1016/j.jcat.2016.06.007>.
- [60] G. Wang, L. Chen, Y. Sun, J. Wu, M. Fu, and D. Ye, "Carbon dioxide hydrogenation to methanol over Cu/ZrO<sub>2</sub>/CNTs: effect of carbon surface chemistry," *RSC Advances*, 10.1039/C5RA04774A vol. 5, no. 56, pp. 45320-45330, 2015, doi: 10.1039/C5RA04774A.
- [61] Y. Sun *et al.*, "Roles of nitrogen species on nitrogen-doped CNTs supported Cu-ZrO<sub>2</sub> system for carbon dioxide hydrogenation to methanol," *Catalysis Today*, vol. 307, pp. 212-223, 2018/06/01/ 2018, doi: <https://doi.org/10.1016/j.cattod.2017.04.017>.
- [62] V. Deerattrakul, P. Puengampholsrisook, W. Limphirat, and P. Kongkachuichay, "Characterization of supported Cu-Zn/graphene aerogel catalyst for direct CO<sub>2</sub> hydrogenation to methanol: Effect of hydrothermal temperature on graphene aerogel synthesis," *Catalysis Today*, vol. 314, pp. 154-163, 2018/09/15/ 2018, doi: <https://doi.org/10.1016/j.cattod.2017.12.010>.
- [63] C. Tisseraud *et al.*, "The Cu–ZnO synergy in methanol synthesis from CO<sub>2</sub>, Part 2: Origin of the methanol and CO selectivities explained by experimental studies and a sphere contact quantification model in randomly packed binary mixtures on Cu–ZnO coprecipitate catalysts," *Journal of Catalysis*, vol. 330, pp. 533-544, 2015/10/01/ 2015, doi: <https://doi.org/10.1016/j.jcat.2015.04.035>.
- [64] S. A. Kondrat *et al.*, "The effect of sodium species on methanol synthesis and water–gas shift Cu/ZnO catalysts: utilising high purity zincian georgeite," *Faraday Discussions*, 10.1039/C6FD00202A vol. 197, no. 0, pp. 287-307, 2017, doi: 10.1039/C6FD00202A.
- [65] S. Xiao *et al.*, "Highly efficient Cu-based catalysts via hydrotalcite-like precursors for CO<sub>2</sub> hydrogenation to methanol," *Catalysis Today*, vol. 281, pp. 327-336, 2017/03/01/ 2017, doi: <https://doi.org/10.1016/j.cattod.2016.02.004>.
- [66] K. C. Waugh, "Methanol Synthesis," *Catalysis Letters*, vol. 142, no. 10, pp. 1153-1166, 2012/10/01 2012, doi: 10.1007/s10562-012-0905-2.
- [67] X. Liu *et al.*, "Selective transformation of carbon dioxide into lower olefins with a bifunctional catalyst composed of ZnGa<sub>2</sub>O<sub>4</sub> and SAPO-34," *Chemical Communications*, Article vol. 54, no. 2, pp. 140-143, 2017, doi: 10.1039/c7cc08642c.
- [68] H. Song, D. Laudenschleger, J. J. Carey, H. Ruland, M. Nolan, and M. Muhler, "Spinel-Structured ZnCr<sub>2</sub>O<sub>4</sub> with Excess Zn Is the Active ZnO/Cr<sub>2</sub>O<sub>3</sub> Catalyst for High-Temperature



Methanol Synthesis," *ACS Catalysis*, vol. 7, no. 11, pp. 7610-7622, 2017/11/03 2017, doi: 10.1021/acscatal.7b01822.

[69] J. Wang *et al.*, "A highly selective and stable ZnO-ZrO<sub>2</sub> solid solution catalyst for CO<sub>2</sub> hydrogenation to methanol," *Science Advances*, vol. 3, no. 10, p. e1701290, 2017, doi: 10.1126/sciadv.1701290.

[70] O. Martin *et al.*, "Indium Oxide as a Superior Catalyst for Methanol Synthesis by CO<sub>2</sub> Hydrogenation," *Angewandte Chemie International Edition*, vol. 55, no. 21, pp. 6261-6265, 2016, doi: 10.1002/anie.201600943.

[71] J. Ye, C. Liu, D. Mei, and Q. Ge, "Active Oxygen Vacancy Site for Methanol Synthesis from CO<sub>2</sub> Hydrogenation on In<sub>2</sub>O<sub>3</sub>(110): A DFT Study," *ACS Catalysis*, vol. 3, no. 6, pp. 1296-1306, 2013/06/07 2013, doi: 10.1021/cs400132a.

[72] P. Gao *et al.*, "Direct conversion of CO<sub>2</sub> into liquid fuels with high selectivity over a bifunctional catalyst," *Nature Chemistry*, Article vol. 9, p. 1019, 06/12/online 2017, doi: 10.1038/nchem.2794

<https://www.nature.com/articles/nchem.2794#supplementary-information>.

[73] P. Gao *et al.*, "Direct Production of Lower Olefins from CO<sub>2</sub> Conversion via Bifunctional Catalysis," *ACS Catalysis*, vol. 8, no. 1, pp. 571-578, 2018/01/05 2018, doi: 10.1021/acscatal.7b02649.

[74] H. Bahruji *et al.*, "Pd/ZnO catalysts for direct CO<sub>2</sub> hydrogenation to methanol," *Journal of Catalysis*, vol. 343, pp. 133-146, 2016/11/01/ 2016, doi: <https://doi.org/10.1016/j.jcat.2016.03.017>.

[75] H. Bahruji *et al.*, "PdZn catalysts for CO<sub>2</sub> hydrogenation to methanol using chemical vapour impregnation (CVI)," *Faraday Discussions*, 10.1039/C6FD00189K vol. 197, no. 0, pp. 309-324, 2017, doi: 10.1039/C6FD00189K.

[76] J. Díez-Ramírez, P. Sánchez, A. Rodríguez-Gómez, J. L. Valverde, and F. Dorado, "Carbon Nanofiber-Based Palladium/Zinc Catalysts for the Hydrogenation of Carbon Dioxide to Methanol at Atmospheric Pressure," *Industrial & Engineering Chemistry Research*, vol. 55, no. 12, pp. 3556-3567, 2016/03/30 2016, doi: 10.1021/acs.iecr.6b00170.

[77] J. Díez-Ramírez, J. A. Díaz, P. Sánchez, and F. Dorado, "Optimization of the Pd/Cu ratio in Pd-Cu-Zn/SiC catalysts for the CO<sub>2</sub> hydrogenation to methanol at atmospheric pressure," *Journal of CO<sub>2</sub> Utilization*, vol. 22, pp. 71-80, 2017/12/01/ 2017, doi: <https://doi.org/10.1016/j.jcou.2017.09.012>.

- [78] Y. Hartadi, D. Widmann, and R. J. Behm, "Methanol formation by CO<sub>2</sub> hydrogenation on Au/ZnO catalysts – Effect of total pressure and influence of CO on the reaction characteristics," *Journal of Catalysis*, vol. 333, pp. 238-250, 2016/01/01/ 2016, doi: <https://doi.org/10.1016/j.jcat.2015.11.002>.
- [79] J. Qu, X. Zhou, F. Xu, X.-Q. Gong, and S. C. E. Tsang, "Shape Effect of Pd-Promoted Ga<sub>2</sub>O<sub>3</sub> Nanocatalysts for Methanol Synthesis by CO<sub>2</sub> Hydrogenation," *The Journal of Physical Chemistry C*, vol. 118, no. 42, pp. 24452-24466, 2014/10/23 2014, doi: 10.1021/jp5063379.
- [80] C. Liu and P. Liu, "Mechanistic Study of Methanol Synthesis from CO<sub>2</sub> and H<sub>2</sub> on a Modified Model Mo<sub>6</sub>S<sub>8</sub> Cluster," *ACS Catalysis*, vol. 5, no. 2, pp. 1004-1012, 2015/02/06 2015, doi: 10.1021/cs501354b.
- [81] Y. Chen, S. Choi, and L. T. Thompson, "Low temperature CO<sub>2</sub> hydrogenation to alcohols and hydrocarbons over Mo<sub>2</sub>C supported metal catalysts," *Journal of Catalysis*, vol. 343, pp. 147-156, 2016/11/01/ 2016, doi: <https://doi.org/10.1016/j.jcat.2016.01.016>.
- [82] I. Sharafutdinov *et al.*, "Intermetallic compounds of Ni and Ga as catalysts for the synthesis of methanol," *Journal of Catalysis*, vol. 320, pp. 77-88, 2014/12/01/ 2014, doi: <https://doi.org/10.1016/j.jcat.2014.09.025>.
- [83] F. Studt *et al.*, "Discovery of a Ni-Ga catalyst for carbon dioxide reduction to methanol," *Nature Chemistry*, Article vol. 6, p. 320, 03/02/online 2014, doi: 10.1038/nchem.1873  
<https://www.nature.com/articles/nchem.1873#supplementary-information>.
- [84] A. R. Richard and M. Fan, "Low-Pressure Hydrogenation of CO<sub>2</sub> to CH<sub>3</sub>OH Using Ni-In-Al/SiO<sub>2</sub> Catalyst Synthesized via a Phyllosilicate Precursor," *ACS Catalysis*, vol. 7, no. 9, pp. 5679-5692, 2017/09/01 2017, doi: 10.1021/acscatal.7b00848.
- [85] A. García-Trenco, A. Regoutz, E. R. White, D. J. Payne, M. S. P. Shaffer, and C. K. Williams, "PdIn intermetallic nanoparticles for the Hydrogenation of CO<sub>2</sub> to Methanol," *Applied Catalysis B: Environmental*, vol. 220, pp. 9-18, 2018/01/01/ 2018, doi: <https://doi.org/10.1016/j.apcatb.2017.07.069>.
- [86] A. Vaccari, "Clays and catalysis: a promising future," *Applied Clay Science*, vol. 14, no. 4, pp. 161-198, 1999/04/01/ 1999, doi: [https://doi.org/10.1016/S0169-1317\(98\)00058-1](https://doi.org/10.1016/S0169-1317(98)00058-1).
- [87] D. Waller, D. Stirling, F. S. Stone, and M. S. Spencer, "Copper–zinc oxide catalysts. Activity in relation to precursor structure and morphology," *Faraday Discussions of the*

*Chemical Society*, 10.1039/DC9898700107 vol. 87, no. 0, pp. 107-120, 1989, doi: 10.1039/DC9898700107.

[88] S. Patel and K. K. Pant, "Influence of preparation method on performance of Cu(Zn)(Zr)-alumina catalysts for the hydrogen production via steam reforming of methanol," *Journal of Porous Materials*, vol. 13, no. 3, pp. 373-378, 2006/08/01 2006, doi: 10.1007/s10934-006-8033-2.

[89] S. Velu, K. Suzuki, and C. S. Gopinath, "Photoemission and in Situ XRD Investigations on CuCoZnAl-Mixed Metal Oxide Catalysts for the Oxidative Steam Reforming of Methanol," *The Journal of Physical Chemistry B*, vol. 106, no. 49, pp. 12737-12746, 2002/12/01 2002, doi: 10.1021/jp021003w.

[90] F. Cavani, F. Trifirò, and A. Vaccari, "Hydrotalcite-type anionic clays: Preparation, properties and applications," *Catalysis Today*, vol. 11, no. 2, pp. 173-301, 1991/12/02/ 1991, doi: [https://doi.org/10.1016/0920-5861\(91\)80068-K](https://doi.org/10.1016/0920-5861(91)80068-K).

[91] L. Zhang, F. Li, D. G. Evans, and X. Duan, "Structure and surface characteristics of Cu-based composite metal oxides derived from layered double hydroxides," *Materials Chemistry and Physics*, vol. 87, no. 2, pp. 402-410, 2004/10/15/ 2004, doi: <https://doi.org/10.1016/j.matchemphys.2004.06.010>.

[92] P. Gao *et al.*, "Influence of modifier (Mn, La, Ce, Zr and Y) on the performance of Cu/Zn/Al catalysts via hydrotalcite-like precursors for CO<sub>2</sub> hydrogenation to methanol," *Applied Catalysis A: General*, vol. 468, pp. 442-452, 2013/11/05/ 2013, doi: <https://doi.org/10.1016/j.apcata.2013.09.026>.

[93] P. Gao *et al.*, "Influence of Zr on the performance of Cu/Zn/Al/Zr catalysts via hydrotalcite-like precursors for CO<sub>2</sub> hydrogenation to methanol," *Journal of Catalysis*, vol. 298, pp. 51-60, 2013/02/01/ 2013, doi: <https://doi.org/10.1016/j.jcat.2012.10.030>.

[94] X. Guo, D. Mao, G. Lu, S. Wang, and G. Wu, "The influence of La doping on the catalytic behavior of Cu/ZrO<sub>2</sub> for methanol synthesis from CO<sub>2</sub> hydrogenation," *Journal of Molecular Catalysis A: Chemical*, vol. 345, no. 1, pp. 60-68, 2011/07/05/ 2011, doi: <https://doi.org/10.1016/j.molcata.2011.05.019>.

[95] F. Arena *et al.*, "Solid-state interactions, adsorption sites and functionality of Cu-ZnO/ZrO<sub>2</sub> catalysts in the CO<sub>2</sub> hydrogenation to CH<sub>3</sub>OH," *Applied Catalysis A: General*, vol. 350, no. 1, pp. 16-23, 2008/11/15/ 2008, doi: <https://doi.org/10.1016/j.apcata.2008.07.028>.

[96] L. H. Zhang, C. Zheng, F. Li, D. G. Evans, and X. Duan, "Copper-containing mixed metal oxides derived from layered precursors: control of their compositions and catalytic

properties," *Journal of Materials Science*, vol. 43, no. 1, pp. 237-243, 2008/01/01 2008, doi: 10.1007/s10853-007-2167-8.

[97] A. Alejandre, F. Medina, P. Salagre, X. Correig, and J. E. Sueiras, "Preparation and Study of Cu–Al Mixed Oxides via Hydrotalcite-like Precursors," *Chemistry of Materials*, vol. 11, no. 4, pp. 939-948, 1999/04/01 1999, doi: 10.1021/cm980500f.

[98] G. Busca *et al.*, "Methanol steam reforming over ex-hydrotalcite Cu–Zn–Al catalysts," *Applied Catalysis A: General*, vol. 310, pp. 70-78, 2006/08/17/ 2006, doi: <https://doi.org/10.1016/j.apcata.2006.05.028>.

[99] Z. Gu, J. J. Atherton, and Z. P. Xu, "Hierarchical layered double hydroxide nanocomposites: structure, synthesis and applications," *Chemical Communications*, 10.1039/C4CC07715F vol. 51, no. 15, pp. 3024-3036, 2015, doi: 10.1039/C4CC07715F.

[100] P. Gao *et al.*, "Effect of hydrotalcite-containing precursors on the performance of Cu/Zn/Al/Zr catalysts for CO<sub>2</sub> hydrogenation: Introduction of Cu<sup>2+</sup> at different formation stages of precursors," *Catalysis Today*, vol. 194, no. 1, pp. 9-15, 2012, doi: 10.1016/j.cattod.2012.06.012.

[101] H. L. Huynh, "Synthesis, characterization, and activity of bimetallic Ni-Fe hydrotalcite-derived catalysts in dry reforming of methane," Z. Yu, Ed., ed: University of Stavanger, Norway, 2018.

[102] Z. P. Xu and P. S. Braterman, "Competitive Intercalation of Sulfonates into Layered Double Hydroxides (LDHs): the Key Role of Hydrophobic Interactions," *The Journal of Physical Chemistry C*, vol. 111, no. 10, pp. 4021-4026, 2007, doi: 10.1021/jp0683723.

[103] A. Bhattacharyya, "Method of hydrocarbon reforming and catalyst precursor," *United States Patent 6071433*, 2000 1998. [Online]. Available: <https://patents.google.com/patent/US6071433A/en>.

[104] Z. P. Xu and G. Q. Lu, "Hydrothermal Synthesis of Layered Double Hydroxides (LDHs) from Mixed MgO and Al<sub>2</sub>O<sub>3</sub>: LDH Formation Mechanism," *Chemistry of Materials*, vol. 17, no. 5, pp. 1055-1062, 2005/03/01 2005, doi: 10.1021/cm048085g.

[105] R. T. Wang, X. P. Liang, Y. Peng, X. W. Fan, and J. X. Li, *Effect of the reaction temperature on nanocrystallites MgAl<sub>2</sub>O<sub>4</sub> spinel ceramic precursor*. 2009, pp. 780-782.

[106] T. S. Srivatsan, "Characterization of Minerals, Metals and Materials", edited by Jiann-Yang Hwang, S.N. Monteiro, Chen Guang Bai, John Carpenter, Mingdong Cai, Donato Firrao, and Byoung-Gon Kim: Wiley (A John Wiley & Sons, Inc.) and TMS, 2012, 531 pp., ISBN 978-1118-291221," *Materials and Manufacturing Processes*, vol. 29, no. 7, pp. 885-885, 2014, doi: 10.1080/10426914.2014.905026.

- [107] B. D. Cullity, *Elements of X-ray diffraction*. Reading, Mass.: Addison-Wesley Pub. Co. (in English), 1956.
- [108] U. Holzwarth and N. Gibson, *The Scherrer equation versus the 'Debye-Scherrer equation'*. 2011, p. 534.
- [109] I. Jendrzewska, P. Zajdel, E. Pietrasik, Z. Barsova, and T. Goryczka, "Application of X-ray powder diffraction and differential scanning calorimetry for identification of counterfeit drugs," (in eng), *Monatshefte fur chemie*, vol. 149, no. 5, pp. 977-985, 2018, doi: 10.1007/s00706-018-2193-z.
- [110] "Chapter 11 Temperature programmed reduction and sulphiding," in *Studies in Surface Science and Catalysis*, vol. 79, J. A. Moulijn, P. W. N. M. van Leeuwen, and R. A. van Santen Eds.: Elsevier, 1993, pp. 401-417.
- [111] A. Auroux, "Calorimetry and thermal methods in catalysis," (in English), 2013. [Online]. Available: <http://public.eblib.com/choice/publicfullrecord.aspx?p=1466657>.
- [112] S. S. Lowell, J. E. Shields, M. Thomas, and M. Thommes, *Characterization of Porous Solids and Powders: Surface Area, Pore Size and Density*. 2006.
- [113] K. Sing *et al.*, "Reporting Physisorption Data for Gas/Solid System," vol. 57, 2008.
- [114] E. P. Barrett, L. G. Joyner, and P. P. Halenda, "The Determination of Pore Volume and Area Distributions in Porous Substances. I. Computations from Nitrogen Isotherms," *Journal of the American Chemical Society*, vol. 73, no. 1, pp. 373-380, 1951/01/01 1951, doi: 10.1021/ja01145a126.
- [115] P. Bedson, E. Prichard, and S. Royal Society of Chemistry, *Gas Chromatography*. Cambridge, UNITED KINGDOM: Royal Society of Chemistry, 2003.
- [116] W. E. Acree, "Basic Gas Chromatography (McNair, Harold M.; Miller, James M.)," *Journal of Chemical Education*, vol. 75, no. 9, p. 1094, 1998/09/01 1998, doi: 10.1021/ed075p1094.
- [117] J.-F. Portha *et al.*, "Kinetics of Methanol Synthesis from Carbon Dioxide Hydrogenation over Copper–Zinc Oxide Catalysts," *Industrial & Engineering Chemistry Research*, vol. 56, no. 45, pp. 13133-13145, 2017/11/15 2017, doi: 10.1021/acs.iecr.7b01323.
- [118] K. M. Vandenbussche and G. Froment, *A steady-state kinetic model for methanol synthesis and the water gas shift reaction on a commercial Cu/ZnO/Al<sub>2</sub>O<sub>3</sub> catalyst*. 1996.
- [119] N. Park, M.-J. Park, Y.-J. Lee, K.-S. Ha, and K.-W. Jun, "Kinetic modeling of methanol synthesis over commercial catalysts based on three-site adsorption," *Fuel Processing Technology* \$V 125, pp. 139-147, 2014.

- [120] T. S. Askgaard, J. K. Norskov, C. V. Ovesen, and P. Stoltze, *A Kinetic Model of Methanol Synthesis*. 1995, pp. 229-242.
- [121] K. Kobl, S. Thomas, Y. Zimmermann, K. Parkhomenko, and A.-C. Roger, "Power-law kinetics of methanol synthesis from carbon dioxide and hydrogen on copper–zinc oxide catalysts with alumina or zirconia supports," *Catalysis Today*, vol. 270, pp. 31-42, 2016/07/15/ 2016, doi: <https://doi.org/10.1016/j.cattod.2015.11.020>.
- [122] L. C. Grabow and M. Mavrikakis, "Mechanism of Methanol Synthesis on Cu through CO<sub>2</sub> and CO Hydrogenation," *ACS Catalysis*, vol. 1, no. 4, pp. 365-384, 2011/04/01 2011, doi: 10.1021/cs200055d.
- [123] E. L. Kunkes, F. Studt, F. Abild-Pedersen, R. Schlögl, and M. Behrens, "Hydrogenation of CO<sub>2</sub> to methanol and CO on Cu/ZnO/Al<sub>2</sub>O<sub>3</sub>: Is there a common intermediate or not?," *Journal of Catalysis*, vol. 328, pp. 43-48, 2015/08/01/ 2015, doi: <https://doi.org/10.1016/j.jcat.2014.12.016>.
- [124] G. H. Graaf, H. Scholtens, E. J. Stamhuis, and A. A. C. M. Beenackers, "Intra-particle diffusion limitations in low-pressure methanol synthesis," *Chemical Engineering Science*, vol. 45, no. 4, pp. 773-783, 1990/01/01/ 1990, doi: [https://doi.org/10.1016/0009-2509\(90\)85001-T](https://doi.org/10.1016/0009-2509(90)85001-T).
- [125] G. H. Graaf, P. J. J. M. Sijtsema, E. J. Stamhuis, and G. E. H. Joosten, "Chemical equilibria in methanol synthesis," *Chemical Engineering Science*, vol. 41, no. 11, pp. 2883-2890, 1986/01/01/ 1986, doi: [https://doi.org/10.1016/0009-2509\(86\)80019-7](https://doi.org/10.1016/0009-2509(86)80019-7).
- [126] G. H. Graaf, E. J. Stamhuis, and A. A. C. M. Beenackers, "Kinetics of low-pressure methanol synthesis," *Chemical Engineering Science*, vol. 43, no. 12, pp. 3185-3195, 1988/01/01/ 1988, doi: [https://doi.org/10.1016/0009-2509\(88\)85127-3](https://doi.org/10.1016/0009-2509(88)85127-3).
- [127] C. V. Ovesen *et al.*, "A Microkinetic Analysis of the Water–Gas Shift Reaction under Industrial Conditions," *Journal of Catalysis*, vol. 158, no. 1, pp. 170-180, 1996/01/01/ 1996, doi: <https://doi.org/10.1006/jcat.1996.0016>.
- [128] M. Peter, M. B. Fichtl, H. Ruland, S. Kaluza, M. Muhler, and O. Hinrichsen, "Detailed kinetic modeling of methanol synthesis over a ternary copper catalyst," *Chemical Engineering Journal*, vol. 203, pp. 480-491, 2012/09/01/ 2012, doi: <https://doi.org/10.1016/j.cej.2012.06.066>.
- [129] L. Stanisław, N. Lech, P. Jerzy, N. Jarosław, K. Paweł, and G. Andrzej, "KINETIC CHARACTERISATION OF CATALYSTS FOR METHANOL SYNTHESIS," (in English), *Chemical and Process Engineering*, vol. 34, no. 4, pp. 497-506, 2013, doi: <https://doi.org/10.2478/cpe-2013-0040>.

- [130] G. M. Schneider, "J. M. Prausnitz: Molecular Thermodynamics of Fluid Phase Equilibria. International Series in the Physical and Chemical Engineering Sciences. Prentice-Hall Inc., Englewood Cliffs, New Jersey, 1969. 523 Seiten Preis: 145 s," *Berichte der Bunsengesellschaft für physikalische Chemie*, vol. 74, no. 3, pp. 308-308, 1970, doi: 10.1002/bbpc.19700740327.
- [131] Z.-M. Hu, K. Takahashi, and H. Nakatsuji, "Mechanism of the hydrogenation of CO<sub>2</sub> to methanol on a Cu(100) surface: dipped adcluster model study," *Surface Science*, vol. 442, no. 1, pp. 90-106, 1999/11/10/ 1999, doi: [https://doi.org/10.1016/S0039-6028\(99\)00900-0](https://doi.org/10.1016/S0039-6028(99)00900-0).
- [132] J. W. Evans, M. S. Wainwright, A. J. Bridgewater, and D. J. Young, "On the determination of copper surface area by reaction with nitrous oxide," *Applied Catalysis*, vol. 7, no. 1, pp. 75-83, 1983/07/15/ 1983, doi: [https://doi.org/10.1016/0166-9834\(83\)80239-5](https://doi.org/10.1016/0166-9834(83)80239-5).
- [133] P. Gao *et al.*, "Cu/Zn/Al/Zr catalysts via phase-pure hydrotalcite-like compounds for methanol synthesis from carbon dioxide," *Journal of CO<sub>2</sub> Utilization*, vol. 11, pp. 41-48, 2015, doi: 10.1016/j.jcou.2014.12.008.
- [134] R. T. Shannon and C. T. Prewitt, "Effective ionic radii in oxides and fluorides," *Acta Crystallographica Section B: Structural Crystallography and Crystal Chemistry*, vol. 25, no. 5, pp. 925-946, 1969.
- [135] S. Velu, D. P. Sabde, N. Shah, and S. Sivasanker, "New Hydrotalcite-like Anionic Clays Containing Zr<sup>4+</sup> in the Layers: Synthesis and Physicochemical Properties," *Chemistry of Materials*, vol. 10, no. 11, pp. 3451-3458, 1998/11/01 1998, doi: 10.1021/cm980185x.
- [136] L. H. Zhang, F. Li, D. G. Evans, and X. Duan, "Cu–Zn–(Mn)–(Fe)–Al Layered Double Hydroxides and Their Mixed Metal Oxides: Physicochemical and Catalytic Properties in Wet Hydrogen Peroxide Oxidation of Phenol," *Industrial & Engineering Chemistry Research*, vol. 49, no. 13, pp. 5959-5968, 2010/07/07 2010, doi: 10.1021/ie9019193.
- [137] M. Thommes *et al.*, "Physisorption of gases, with special reference to the evaluation of surface area and pore size distribution (IUPAC Technical Report)," in *Pure and Applied Chemistry* vol. 87, ed, 2015, p. 1051.
- [138] Y. Amenomiya, "Methanol synthesis from CO<sub>2</sub> + H<sub>2</sub> II. Copper-based binary and ternary catalysts," *Applied Catalysis*, vol. 30, no. 1, pp. 57-68, 1987/03/16/ 1987, doi: [https://doi.org/10.1016/S0166-9834\(00\)81011-8](https://doi.org/10.1016/S0166-9834(00)81011-8).
- [139] C. Tisseraud, C. Comminges, S. Pronier, Y. Pouilloux, and A. Le Valant, "The Cu–ZnO synergy in methanol synthesis Part 3: Impact of the composition of a selective Cu@ZnOx core–shell catalyst on methanol rate explained by experimental studies and a concentric spheres

model," *Journal of Catalysis*, vol. 343, pp. 106-114, 2016/11/01/ 2016, doi:  
<https://doi.org/10.1016/j.jcat.2015.12.005>.



# APPENDIX A: CALCULATIONS OF CATALYSTS SYNTHESIS

## Un-Promoted Catalysts

Hydrotalcite catalyst has the following formula  $[M^{2+}_{1-x}M^{3+}_x(OH)_2]^{x+}(A^{n-})_{x/n}.mH_2O$ . The catalyst must contain Cu/ZnO/Al<sub>2</sub>O<sub>3</sub>-In<sub>2</sub>O<sub>3</sub> after calcination and reduction. The compositions are calculated as follows. Define  $a = \text{mol of Cu}^{2+}$ ,  $b = \text{mol of Zn}^{2+}$ ,  $c = \text{mol of Al}^{3+}$ .

$$\frac{M^{2+}}{M^{3+}} = \frac{a + b}{c} = 3$$

Thus, the trivalent ionic ration  $x$  was chosen to be 0.25, which aligns perfectly between 0.2 and 0.4 to guaranty the formation of a hydrotalcite structure. The following is obtained:

$$x = c = 0.25$$

$$1 - x = a + b = 0.75$$

Molar ratio of  $\text{Cu}^{2+}/\text{Zn}^{2+}$  was taken as 1.5, 1, 0.5. Stoichiometric coefficients are listed in Table A 1 below:

Table A 1. Stoichiometric coefficients of CuZnAl catalysts

Sample	$\text{Cu}^{2+}$	$\text{Zn}^{2+}$	$\text{Al}^{3+}$	$\text{OH}^-$	$\text{CO}_3^{2-}$
1.5-CuZnAl	0.09	0.06	0.05	0.4	0.025
1-CuZnAl	0.075	0.075	0.05	0.4	0.025
0.5-CuZnAl	0.05	0.1	0.05	0.4	0.025

In co-precipitation conventional synthesis method, the total metal concentration of 400-mL metal nitrate solution was 0.5 M. The amount of Na<sub>2</sub>CO<sub>3</sub> was doubled to insure pillaring. Mass of reactants are listed in Table A 2 below:

Table A 2. Mass of salts used

Samples	$\text{Cu}(\text{NO}_3)_2 \cdot x_3 \text{H}_2\text{O}$	$\text{Zn}(\text{NO}_3)_2 \cdot x_6 \text{H}_2\text{O}$	$\text{Al}(\text{NO}_3)_3 \cdot 9 \text{H}_2\text{O}$	NaOH	Na <sub>2</sub> CO <sub>3</sub>	Needed Na <sub>2</sub> CO <sub>3</sub>
1.5-CuZnAl	26.1927	11.8176	18.7565	16	2.64975	5.2995
1-CuZnAl	21.82725	14.772	18.7565	16	2.64975	5.2995
0.5-CuZnAl	14.5515	19.696	18.7565	16	2.64975	5.2995

## Promoted Catalysts

Similarly, define  $a = \text{mol of Cu}^{2+}$ ,  $b = \text{mol of Zn}^{2+}$ ,  $c = \text{mol of Al}^{3+}$ , and  $d = \text{mol of In}^{3+}$ .

$$\frac{M^{2+}}{M^{3+}} = \frac{a + b}{c + d} = 3$$

Thus, the trivalent ionic ration  $x$  was chosen to be 0.25, which aligns perfectly between 0.2 and 0.4 to guaranty the formation of a hydrotalcite structure. The following is obtained:

$$x = c + d = 0.25$$

$$1 - x = a + b = 0.75$$

Molar ratio of  $\text{Cu}^{2+}/\text{Zn}^{2+}$  was taken as 1. Stoichiometric coefficients are listed in Table A 3 below:

Table A 3. Stoichiometric coefficients of CuZnAl-In catalysts

Sample	$\text{Cu}^{2+}$	$\text{Zn}^{2+}$	$\text{Al}^{3+}$	$\text{In}^{3+}$	$\text{OH}^-$	$\text{CO}_3^{2-}$
1-CuZnAl-0-In	0.075	0.075	0.05	0	0.4	0.025
1-CuZnAl-2.5-In	0.075	0.075	0.045	0.005	0.4	0.025
1-CuZnAl-5-In	0.075	0.075	0.04	0.01	0.4	0.025
1-CuZnAl-7.5-In	0.075	0.075	0.035	0.015	0.4	0.025

In co-precipitation conventional synthesis method, the total metal concentration of 400-mL metal nitrate solution was 0.5 M. The amount of  $\text{Na}_2\text{CO}_3$  was doubled to insure pillaring. Mass of reactants are listed in Table A 4 below:

Table A 4. Mass of salts used

Samples	$\text{Cu}(\text{NO}_3)_2 \times 3\text{H}_2\text{O}$	$\text{Zn}(\text{NO}_3)_2 \times 6\text{H}_2\text{O}$	$\text{Al}(\text{NO}_3)_3 \times 9\text{H}_2\text{O}$	$\text{In}(\text{NO}_3)_3$	NaOH	$\text{Na}_2\text{CO}_3$	Needed $\text{Na}_2\text{CO}_3$
1-CuZnAl-0-In	21.82725	14.772	18.7565	0	16	2.64975	5.2995
1-CuZnAl-2.5-In	21.82725	14.772	16.88085	1.59425	16	2.64975	5.2995
1-CuZnAl-5-In	21.82725	14.772	15.0052	3.1885	16	2.64975	5.2995
2CuZnAl-7.5-In	21.82725	14.772	13.12955	4.78275	16	2.64975	5.2995